Research
Civil Engineering Materials—Review

Steel Fiber–Matrix Interfacial Bond in Ultra-High Performance Concrete: A Review

Yulin Deng [a], Zuhua Zhang [b,*], Caijun Shi [a], Zemei Wu [a], Chaohui Zhang [a]

[a] Key Laboratory for Green & Advanced Civil Engineering Materials and Application Technology of Hunan Province, College of Civil Engineering, Hunan University, Changsha 410082, China
[b] Key Laboratory of Advanced Civil Engineering Materials of Ministry of Education, School of Materials Science and Engineering, Tongji University, Shanghai 201804, China

ARTICLE INFO

ABSTRACT

Ultra-high performance concrete (UHPC) is a relatively new cementitious concrete composite with significant application potential in infrastructure construction because of its excellent mechanical strength and durability. The steel fiber–matrix interfacial bond is the main factor that governs other mechanical properties of UHPC, including tensile, flexural, and compressive strengths and failure mode (fracture behavior). This paper presents a comprehensive review on the research progress of fiber–matrix bond behaviors of UHPC by discussing and comparing a range of fiber pullout testing methods and analytical models. The parameters of the fiber–matrix bond, including the geometry and orientation of fibers, surface treatment, and composition and strength of the matrix, are identified and discussed in detail. Lastly, recommendations for future research related to UHPC strengthening methods and testing details are provided based on recent progress.

© 2022 THE AUTHORS. Published by Elsevier LTD on behalf of Chinese Academy of Engineering and Higher Education Press Limited Company. This is an open access article under the CC BY-NC-ND license (http://creativecommons.org/licenses/by-nc-nd/4.0/).

1. Introduction

Ultra-high performance concrete (UHPC) has gained significant attention and been applied to several fields globally because of its extremely high strength, good toughness, and excellent durability, as shown in Fig. 1 [1]. For architectural works, UHPC is effectively used in the construction of complex structures, such as long-span curved roofs, intricately shaped facades, and green balconies [2]. In engineering, utilization of UHPC prevents the failure of the bridge deck under fatigue load and restrains the concrete cracking in the box beam [3]. Further, UHPC exhibits excellent wear resistance in extreme environments and thus can be effectively used for rapid maintenance of roads and other transport infrastructure. Similarly, the use of UHPC extends the life span and reduces maintenance costs of runways and taxiways in airports. Broader applications of UHPC in furniture and decorative elements, mechanical parts (e.g., windmill tower connection), offshore platforms, and military defense systems have been proposed and proven promising.

In UHPC, fiber is the most important ingredient that alters the fracture mode of plain concrete from brittle to ductile [3]. The addition of discontinuous steel fibers enhances the critical cracking strength and delays the initiation of cracking by reducing the total stress at the crack tip and inhibiting matrix shrinkage [4,5]. In the post-crack stage, fibers also improve the ultimate tensile strength and energy absorption capacity through bridging the cracked parts of UHPC, as shown in Fig. 2 [6]. The fiber-bridging mainly depends on the fiber–matrix interfacial bond.

Fiber–matrix interfacial bond refers to the stress transferring from the surrounding matrix to the fiber at the interface [7]. The bond strength between fiber and matrix affects compressive, flexural, and tensile strengths, along with fracture energy, dynamic response, elastic modulus, ductility, and durability [8–12]. When the bond strength is lower than the tensile strength of the matrix, fibers are pulled out under lower external loads, resulting in the underutilization of the potential strength of composites [13]. In contrast, excessive bond strength leads to a sudden fiber rupture and/or matrix spalling, failing to resist cracks development during pullout. Thus, an understanding of bond failure modes and pullout behaviors is needed to enhance the tensile performance and other mechanical properties of UHPC.

Various experimental methods and theoretical models have been developed to investigate the fiber–matrix bond characteristics of UHPC [14,15]. The pullout test is the most commonly employed experimental method where one end of a pullout specimen is restricted with displacement, and a uniaxial pullout

* Corresponding author.
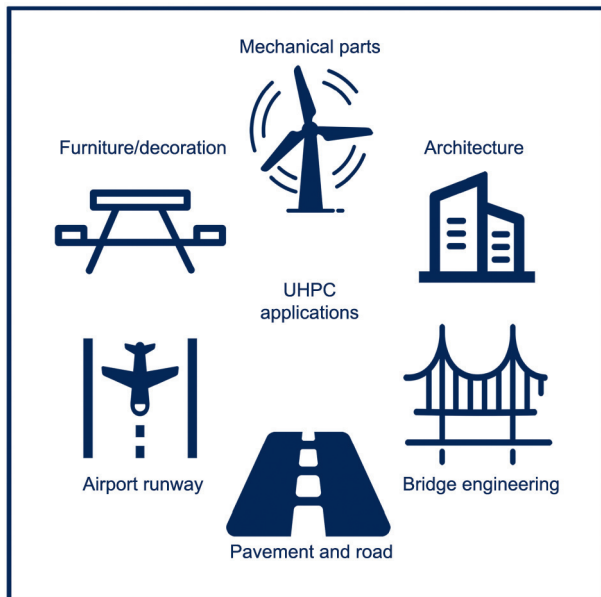   *E-mail address:* zhangzuhua@tongji.edu.cn (Z. Zhang).

Fig. 1. UHPC application fields.

treatment, geometry, and orientation of fiber, and strength and components of the matrix [15,18–20]. Deformed fibers have been widely employed in UHPC because the use of mechanically pre-deformed fibers can significantly increase (three- to seven-fold) the bond properties of UHPC [19]. Moreover, discontinuous fibers are randomly distributed in UHPC. The oblique bridging fibers on the crack leads to an improved pullout resistance as well as a higher fiber rupture and/or local matrix damage potential than the aligned fibers [15]. In addition, a high matrix strength generally improves bond performance in UHPC but may decrease it in some cases [20].

This paper comprehensively reviews the existing literature on the interaction between steel fiber and matrix in UHPC, including bond testing and evaluation methods, bond failure modes, theoretical mechanical analysis models, and factors affecting the bond. This study aimed at developing a comprehensive understating of fiber strengthening and toughening mechanisms in UHPC to provide relevant valuable information for future research.

2. Bond testing methods

Bond testing methods are important for obtaining accurate assessment results. The fiber pullout test is a direct testing methods that can measure fiber–matrix shear strength by simulating the fiber bridge at the cracking site in the matrix. Common pullout testing methods can be divided into single-sided and double-sided methods [21]. Several test procedures have been developed to measure the bond property between the fiber and matrix; however, none of them can meet all testing purposes. Further, mechanical properties, such as tensile and flexural strengths of fiber-reinforced concrete, are usually used as an index for indirect testing methods [22]. Other microstructural analyses might provide indirect evidence of bonding properties, such as micro-hardness measurement of the interface [23]. However, there is no standard indirect method that can be widely adopted for testing the fiber–matrix interfacial bond.

2.1. Pullout testing

Pullout testing is a relatively simple, economical, and feasible method commonly used to measure fiber–matrix bond strength under both static and impact loads. Moreover, the stress conditions between fiber and matrix during pullout testing are theoretically similar to those of bridging fiber and cracking matrix in the cracking process of composite materials [24].
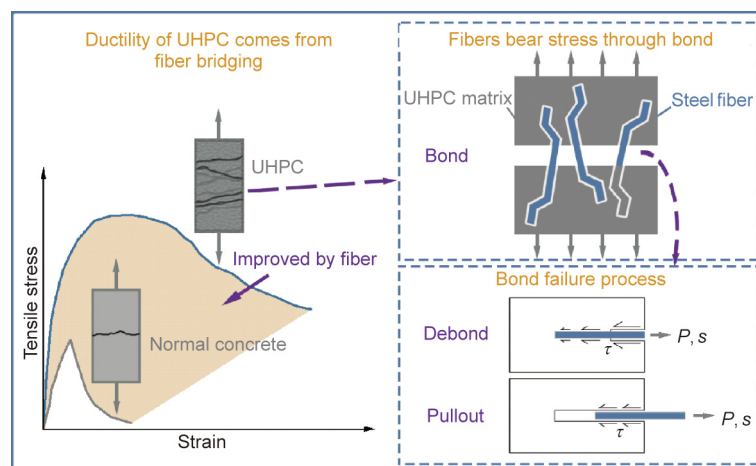
force is applied on the free side of the pullout specimen to assess the bond strength [16]. The free side of the pullout specimen could be the free end of a fiber or the specimen with embedded fiber. According to our research, two widely accepted testing standards—the American Society of Testing Materials (ASTM) and European Norm (EN) standards lack information on test setup details or loading conditions to properly investigate fiber–matrix bond properties, thus making it difficult to quantitatively compare pullout test results from various researchers. Considering that no existing method for pullout test meets all test requirements (e.g., experimental accuracy and preparation efficiency), it is necessary to compare available methods applied for UHPC to find the ways of improving the pullout testing method. Further, to predict pullout test results, various analysis models are adopted because they are generally cost- and time-effective. In theoretical models, fiber–matrix interfacial friction laws are generally assumed to be linear-elastic before debonding [17]. After debonding, the stress–slip relations notably vary with the change in properties of matrix and fiber, particularly the fiber deformation.

In the past few decades, researchers have extensively studied the factors affecting bond properties of UHPC, including surface

Fig. 2. Fiber contribution to UHPC. P, s, and τ are the pullout load, fiber slip, and bond shear stress, respectively.

Based on the tensile force application methods, pullout tests can be classified into two: single-sided and double-sided [25]. Accordingly, based on the number of fibers and methods of applying tensile force, fiber pullout tests can be categorized as follows: ① single fiber in single-sided specimens; ② single fiber in double-sided specimens; ③ multiple fibers in single-sided specimens; and ④ multiple fibers in double-sided specimens. The advantages and disadvantages of these pullout tests are listed in Table 1. The single-fiber single-side pullout test is the most widely applied method because of manufacturing, transportation, and curing ease [26].

The reliability and accuracy of pullout test results can significantly be influenced by sample preparation method, gripping variability, fiber alignment [27], and operational errors (such as inaccurate fiber placement). Consequently, the variation coefficient is usually high ($\geq 30\%$). For the single-fiber test, the utilization of a long fiber embedded in the UHPC matrix and several parallel specimens (more than ten) contribute to relatively high accuracy and reliability of testing results. An acrylic block or a two-piece acrylic fixture with nicks can ensure fiber inclination angle inside a dog bone-shaped mold before pouring the paste [14,28]. The total pullout load of the single-fiber test is generally low, contributing to a high coefficient of variation; therefore, the multiple-fibers test comprising four or nine fibers is adopted when the instrument precision is low. Multiple fibers placed symmetrically in the matrix can significantly improve test accuracy by minimizing eccentricity [29].

It should be noted that the bond strength of one fiber from a single-fiber pullout test can be higher than that from a multiple-fibers test at both static and impact loads [30]. This could be due to two reasons: First, multiple fibers cannot achieve the maximum load at the same time in a multiple-fibers test; second, the local stress and strain concentration of matrix caused by the interphase interaction of multiple fibers.

Following measures should be considered during specimen preparation and test operation to obtain accurate results [16,25,31]:

(1) The embedded fiber length should be placed and measured accurately;

(2) The length of the free part of fiber should keep as short as possible;

(3) The fiber orientation should keep free to change from 0° to 90° relative to the direction of the pullout load;

(4) The specimens should permit the application of secondary loads (e.g., radial and axial compression to the matrix);

(5) To minimize shrinkage and surface drying caused by the shape and size of the specimen, test device, and environment.

Typical pullout test setups that have been adopted for UHPC test are provided in Table 2 [4,14,22,26,32–38].
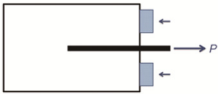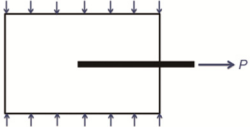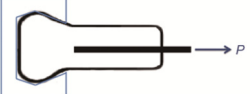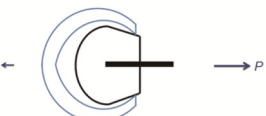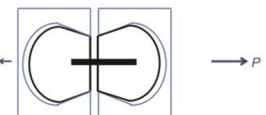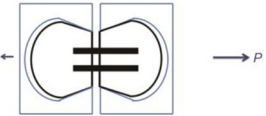
A reliable multiple-fibers double-sided test is required to obtain the bond/rupture strength of fiber embedded in the UHPC matrix. In addition to the benefits of low instrument accuracy requirement and high reliability, as mentioned in Table 1, the application of hybrid fibers makes the multiple-fibers test more practical. Moreover, a double-sided test can effectively simulate the actual debonding and pullout behavior [25]. In contrast, a single-sided test demands an extremely short free end of the fiber to meet the stress and strain conditions during pullout, leading to difficult instrument operation and specimen manufacturing. The double-sided test also avoids stress concentration at the fiber exit point (specifically for inclined fibers) caused by the instrument grip [14]. It should be noted that the gripping and restraint device applied to the matrix should be installed away from the part where fibers are embedded to achieve the desired stress conditions in double-sided tests [21]. Thus, a dog bone-shaped specimen with the ends away from the embedded fiber is a good choice. The double-sided matrixes combined with multiple-fibers test simplify the operation and reduce the number of specimens required to achieve test reliability. ACI 544.9R–2017 [21] summarizes the effect of the test setup and loading conditions on pullout test results; however, ASTM or EN standards do not provide any details for pullout tests. Multiple-fibers double-sided test has been adopted by the Chinese national standard China Association for Engineering Construction Standardization (CECS)-13 [39], in which the test setup is acceptable.

Moreover, it is necessary to ensure fiber alignment during the fabrication of specimens containing inclined fibers. Some modified mold accessories for fixing fiber position or orientation during molding have been applied to improve the manufacturing efficiency and accuracy of fiber alignment. For instance, Kim and Yoo [28] used an acrylic block with a polyvinyl chloride (PVC) sheet for specimen fabrication, as shown in Fig. 3(a). One end of the fiber was bent in the fixed section to ensure that every fiber should be pulled out only from the designed section. A long embedded length of fiber at the fixed end also helped in complete pullout from the pullout side. After being cast on the pullout side, the acrylic block was removed and casted on the fixed side. Lee et al. [26] applied a steel plate and polytheme (PE) sheet for fabricating a double-sided specimen with several fibers, as shown in Fig. 3(b). Tai and El-Tawil [14] designed a two-piece fixed fixture with nicks engraved to ensure fiber alignment, as shown in Fig. 3(c). These accessories are mainly rigid fixtures with/without a sheet. The thin sheet is placed in the middle of the mold, and the thick fixtures are used to hold the fiber position and alignment.

Table 1
Advantages and disadvantages of various pullout testing methods.

Test	Advantages	Disadvantages
Single-fiber test	• Simple and convenient	• Highly precise equipment is required owing to small pullout load • Large variability • Effect of fiber spacing could not be considered
Multiple-fibers test	• Relatively low requirement for equipment precision • Low variability	• Inconvenient operation • Lower pullout load result than that of single-fiber test • Higher possibility of local stress and strain concentration of matrix • Difficult to manufacture an enormous number of specimens safely and rapidly
Single-sided test	• Fiber–matrix interface can be observed directly • Simple and convenient	• Difficulty in gripping the free end of fiber
Double-sided test	• Easy to grasp specimens • Simulating the practical stress/strain conditions of the composites	• Inconvenient operation • Difficult to manufacture an enormous number of specimens safely and rapidly

Table 2
Pullout test procedures for UHPC.

| Specimen	Test configuration	Remarks	Refs.
	Single-fiber, single-sided	A 50 mm × 50 mm × 50 mm or 100 mm × 100 mm × 50 mm specimen was fixed to a frame	[32,33]
		A 10 mm × 10 mm × 10 mm specimen; a compressive stress up to 76 MPa was applied by an active screw to investigate confinement effect	[34]
		Angle up to 45°; two half dog bone-shaped specimens were cast in one modified mold	[14,35,36]
		A round matrix grip was selected to reduce the grip confinement	[4]
	Single-fiber, double-sided	Fiber angle up to 60°	[37]
	Multiple-fibers, double-sided	Four or nine fibers embedded in a dog-bone specimen	[22,38]
		32 fibers embedded in a dog-bone specimen; angle up to 60°	[26]
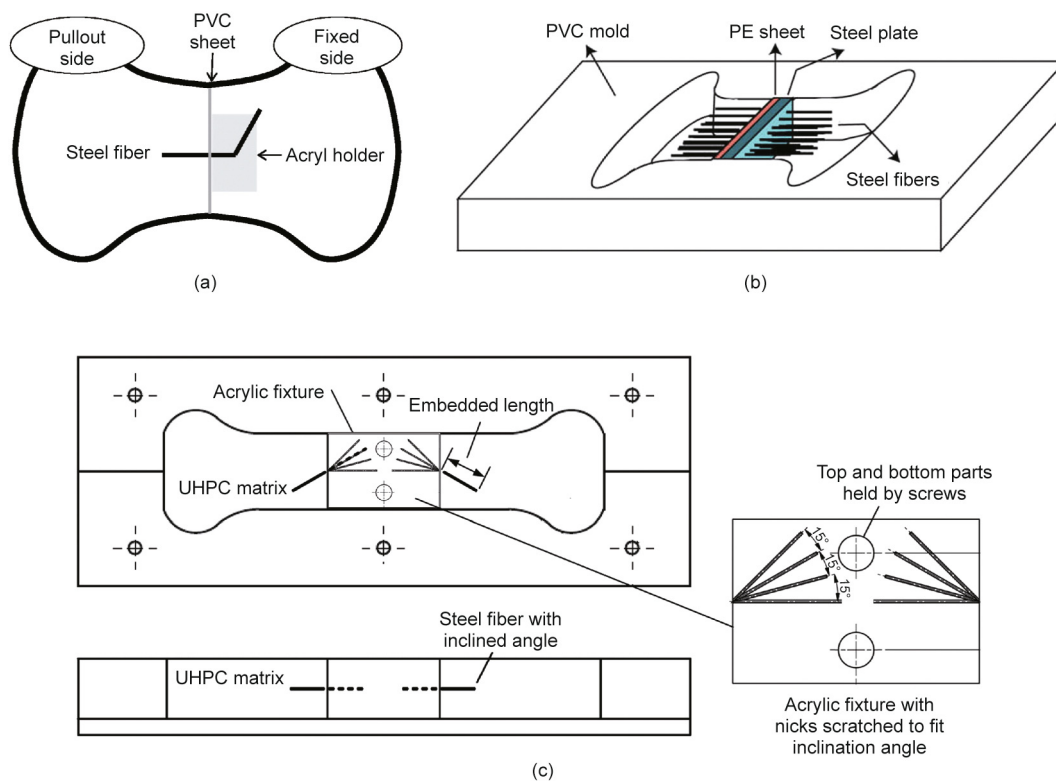
Fig. 3. Mold setups with fiber alignment ensured by: (a) an acrylic block [28], (b) steel plate [26], and (c) two-piece fixed fixture with engraved nicks [14]. PE: polytheme.

However, the effects of fiber volume and fiber distribution characteristics on the bending strength are more significant than that of pullout strength due to stress concentration [5,16]. The variation in fiber volume from 1% to 3% can increase the bending strength of straight fiber by 45%; however, increasing the bond strength up to 650% can only cause an increase of 28% in the bending strength, which is an inefficient method [16]. The disproportionate relationship between the bond performance and tensile behavior indicates that pullout strength should be combined with the volume, orientation, aspect ratio of fibers, and matrix flexural strength. This could be done using the theory of composites or macroscopic finite element model to make the pullout test results more practical for structural design and engineering applications.

2.2. Evaluation indexes of pullout behavior

To evaluate the effect of various parameters on interfacial bond strength, pullout energy, and fiber utilization efficiency, the following mechanical indexes of single-fiber single-sided test have been proposed.

Maximum fiber stress: The maximum fiber stress (or the maximum tensile stress), σ_{max}, is a good measure of the utilization degree of the steel fiber material [36], and can be expressed as follows:

$$\sigma_{max} = \frac{4P_{max}}{\pi d_f^2} \tag{1}$$

where P_{max} is the peak pullout load (N) and d_f is the diameter of the fiber (mm).

Pullout work or energy: The pullout work or energy (W_P) is geometrically defined as the area below the pullout load–slip curve [36], indicating the energy dissipation ability of the single fiber during the pullout process, and can be calculated as follows:

$$W_P = \int_{s=0}^{s=L_E} P(s)\,ds \tag{2}$$

where P is the pullout load (N), s is the fiber slip (mm), and L_E is the initial embedded length of fiber (mm).

Unit pullout work or energy w_P (per embedded fiber surface area): It refers to the pullout work of the unit area of the fiber embedded part, and represents the efficiency of energy absorption.

$$w_P = \frac{W_P}{\pi d_f L_E} \tag{3}$$

Equivalent bond strength: The equivalent bond strength (τ_{eq}) is defined as the average bond strength based on the dissipated energy during fiber pullout:

$$\tau_{eq} = \frac{2W_P}{\pi d_f L_E^2} \tag{4}$$

Average bond strength: The average bond strength (τ_{av}) is the interfacial shear stress when the maximum pullout load is reached, representing the crack resistance ability [36]:

$$\tau_{av} = \frac{P_{max}}{\pi d_f L_E} \tag{5}$$

Actual interfacial shear stress: The actual interfacial shear stress is determined by the pullout load at any slip divided by the current bond surface area as follows [40]:

$$\tau(s) = \frac{P(s)}{\pi d_f (L_E - s)} \tag{6}$$

where $\tau(s)$ is the slip dependent shear stress, averaged over the current embedment length ($L_E - s$), respectively.

To evaluate the bond property under certain variables, more evaluation indexes are expressed as following.

The real slip length. The slip value directly measured from the free section, s_m, cannot represent the real slip of the fiber, since it involves the elastic deformation (only elastic deformation needs to be considered here when the maximum pullout stress for most cases is less than the yielding strength of steel fiber) of the exposed fiber part [40]. Therefore, the actual slip can be expressed by

$$s' = s_m - \frac{PL_0}{EA} \tag{7}$$

where s', L_0, E, and A are the actual slip of the loaded end (mm), length of the exposed fiber part (mm), elastic modulus of the pulled out steel fiber (MPa), and cross sectional area of fiber (mm^2), respectively.

Energy and bond strength indexes considering fiber volume content in matrix: A new energy dissipation index η_f was introduced, which can be calculated by dividing the single fiber pullout work by the fiber volume [41]. Similarly, a new bond strength index ς_f was proposed to evaluate the interfacial bond efficiency, expressed as single fiber average bond strength divided by fiber volume [41]. The two indexes can be expressed as follows:

$$\eta_f = \frac{W_P}{A_f L_f} \tag{8}$$

$$\varsigma_f = \frac{\tau_{av}}{A_f L_f} \tag{9}$$

where A_f and L_f are the sectional area (mm^2) and length of fiber (mm), respectively.

3. Fiber–matrix interfacial bond and failure mode

3.1. Interfacial bond

The mechanism controlling fiber–matrix bond mainly comprises three parts: ① chemical/physical adhesion (physicochemical adhesion); ② friction; ③ mechanical anchorage [7,31]. Generally, physical adhesion is stronger than chemical adhesion because, in general, no chemical reaction occurs between steel fiber and UHPC matrix. Chemical/physical adhesion and friction act at fiber–matrix interface. Mechanical anchorage can substantially affect the bond through interlock (entanglement) between fibers, plastic deformation of the fiber, and additional normal force pressure. The three basic bond mechanisms of fiber embedded in UHPC are the same as those in normal concrete.

The stress transition affects the bond mechanisms. According to the alignment of stress transmitted along the interface relative to the fiber, the fiber–matrix interface bond can be divided into bond shear stress τ (parallel to the interface) and bond tensile stress σ (perpendicular to the interface) [42]. These can be expressed as follows:

$$\tau = \frac{P}{\pi d_f l_E} \tag{10}$$

$$\sigma = \frac{N}{\pi d_f l_E} \tag{11}$$

where l_E and N are the length of fiber in matrix (mm) and normal force (N), respectively.

The pullout and normal forces distributed on an embedded fiber in a cementitious matrix are shown in Fig. 4. Shear bond resists the pullout force and is one of the main factors affecting the mechanical failure behavior of UHPC. Before cracking, the shear bond transfers stress between fiber and matrix. In a cracked UHPC, bridging fibers at the cracking location carry the load, and the
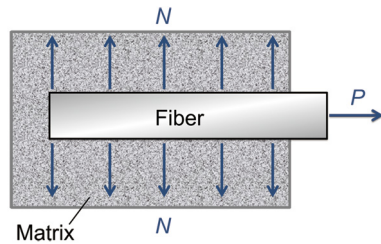
Fig. 4. Illustration of pullout and distributed normal forces on an embedded fiber in a cementitious matrix during fiber pullout.

shear bond transfers stress to the uncracked matrix. Shear bond is generally classified into elastic and friction bonds [43]. When the pullout force is less than the critical pullout force for slipping, elastic bonds assist in safely transferring the stress without debonding or fiber slippage. Once the critical pullout force is reached, the balance is lost, and a relative displacement occurs between fiber and matrix in the axial and peripheral directions. After the failure of elastic bonds, friction bonds are produced, which resist the displacement along the interface parallel to the length of fiber. When the frictional bond exceeds the ultimate elastic shear bond, fiber–matrix debonding develops gradually; however, when the frictional bond strength is lower than that of the ultimate elastic shear bond, a sudden increase in stress can lead to a rapid debonding. The strength of friction bonds is mainly influenced by friction coefficient at fiber–matrix interface, normal force per unit length of fiber, and Poisson's ratio [44].

Tensile bond resists the normal force exerted by the lateral contraction of fibers in the matrix. Under the normal force, a complete debonding occurs immediately when tensile stress exceeds the tensile bond strength. Considering that the tensile bond strength is higher than the transverse strength of matrix or even the transverse splitting strength of fiber, a tensile failure may occur in the adjacent area of matrix or at the cross-section of fiber parallel to the fiber length (the latter is unlikely due to the high transverse strength of fiber).

The microstructure of the interface significantly affects the mechanical properties of a composite because the bond exists at the fiber–matrix interface. For smooth fibers, the bond behavior is primarily influenced by the density of the interfacial transition zone (ITZ) and C–S–H gel through physicochemical adhesion and friction. The ITZ between steel fiber and matrix in UHPC with 28-day compressive strength of 110 MPa is dense and homogeneous because of low water-to-binder (w/b) ratio and large amount of fine materials [45], as the Backscattered scanning electron micrograph (BSEM) image shown in Fig. 5 [46]. Generally, no microcrack is observed around the fiber. However, the interface may still be porous and sensitive to micro-cracks [11] because of the wall
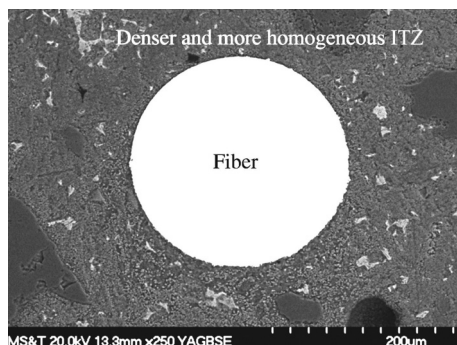

Fig. 5. BSEM image of ITZ between steel fiber and UHPC matrix [46].

and bleeding effect during hydration [47]. The porous zone and micro-cracks at the interface can lead to weak bond strength due to insufficient contact between the fiber and matrix [22]. The properties of the fiber–matrix bond interface can be enhanced by increasing the amount of binder material, reducing w/b ratio, adding supplementary cementitious admixtures, fiber surface treatment, high energy mixing, and improving aggregate and fibers distribution [27,48].

3.2. Fiber bridging and failure mode

In the fiber-bridging and pullout model, a bridging fiber prevents the development of micro-cracking in the matrix and bears tensile stress, particularly after cracking in concrete. The failure mode of fiber bridging is fiber pullout or fiber rupture [37]; matrix spalling can occur in either case. Matrix spalling generally occurs before the pullout or rupture of fiber, and the bond strength is decreased due to severe matrix damage. A significantly stronger bond can lead to sudden fiber rupture and possibly matrix spalling. When the bond stress in a dense ITZ is greater than the ultimate strength of the surrounding matrix, a spalling can be observed. When the bond strength exceeds the ultimate tensile strength of fiber, fiber rupture occurs [49]. Due to the weak fiber–matrix interface and high tensile strength of steel fiber, fiber pullout is the most observed failure mode under loading. The fiber rupture associated with over-utilization of fiber tensile strength and brittle matrix failure should be avoided [41].

In conclusion, fiber-bridging plays a major role in determining the post-cracking behavior of UHPC. Nevertheless, the softening behavior of the matrix in UHPC containing fibers becomes less brittle because fibers change the cracking pattern [50]. Therefore, the contribution of the matrix should also be considered to establish the post-cracking behavior.

3.2.1. Fiber pullout failure mode and pullout behavior

In recent studies, numerous differences in pullout behaviors have been observed for steel fibers with different geometric shapes, such as the pullout load–slip responses of straight, hooded-end, and corrugated fibers in UHPC [19,51]. For straight fibers, adhesion and friction are the two important factors affecting the pullout behavior [40]. Similarly, mechanical anchoring force works together with adhesion and friction for deformed fibers. The pullout behavior of fiber embedded in UHPC and that in normal concrete are compared in detail herein.

(1) **Straight fiber.** Fig. 6(a) shows the representative pullout load–slip curve of a straight smooth fiber divided into four stages: ① elastic (O–P'_{S1}); ② partial debonding (P'_{S1}–P'_{S2}); ③ full debonding (P'_{S2}–P'_{S3}); ④ pullout (slipping) (P'_{S3}–S'). O is the point at which the fiber begins to bear pullout load. P'_{S1} represents the pullout load value at the beginning of debonding. P'_{S2} is the maximum pullout load. P'_{S3} is pullout load when the fiber sliding starts. S' refers to the state of the fiber just out of the cement matrix. Δ_{S1}, Δ_{S2}, and Δ_{S3} are the corresponding slip of the fiber when pullout load reaches P'_{S1}, P'_{S2}, and P'_{S3}, respectively. At stage ①, physical adhesion restrains the pullout of fiber. During stages ②–③, the adhesion in bonded area collaborates with friction in the debonded area. While at stage ④, the fiber must overcome kinetic friction only because there is no mechanical anchorage. Debonding (including partial and fully debonding) and dynamic friction sliding are the major stages when fibers are pulled out [52].

Initially, the pullout load increases linearly with slip in the elastic stage. With the initiation of macro-cracking, the debonding along the fiber–matrix interface occurs and continues to develop from the pullout end to the embedded end. Then the load is rapidly increased to the peak load (P'_{S2}) at the point where only a short part of the fiber is bonded. Due to the high friction and denser
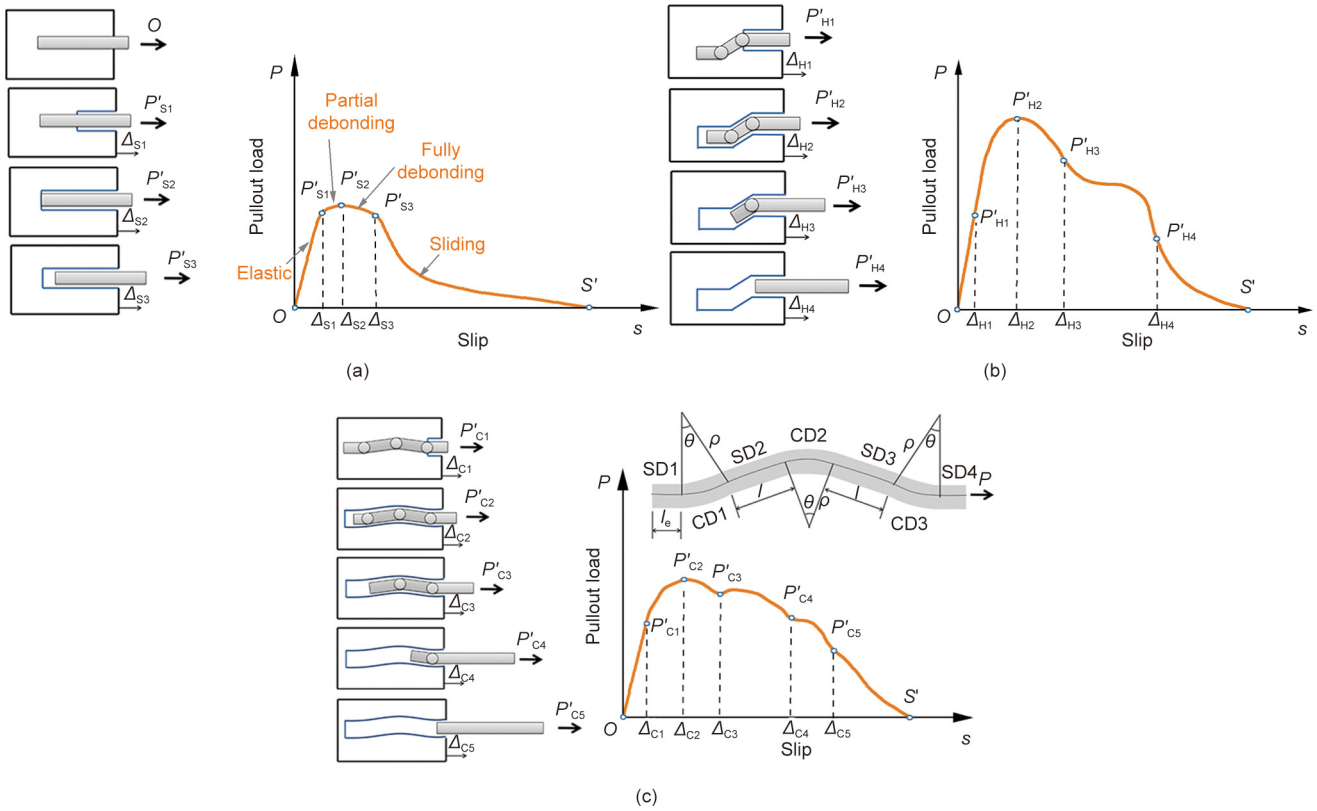
Fig. 6. Pullout behavior of (a) straight, (b) hooked, and (c) corrugated fibers. Straight duct (SD) and curved duct (CD) are the ducts where corrugated steel fiber is embedded. O: the point at which the fiber begins to bear pullout load; P'_{S1}: the pullout load value at the beginning of debonding; P'_{S2}: the maximum pullout load; P'_{S3}: pullout load when the fiber sliding starts; S': the state of the fiber just out of the cement matrix; Δ_{S1}, Δ_{S2}, and Δ_{S3}: the corresponding slip of the fiber when pullout load reaches P'_{S1}, P'_{S2}, and P'_{S3}, respectively; P'_{H1}: the pullout load when the fiber is completely debonded; P'_{H2}: the first plateau load due to the contribution of two plastic hinges; P'_{H3}: the second plateau load when only one plastic hinge works in matrix; P'_{H4}: the pullout load without plastic hinge; Δ_{H1}, Δ_{H2}, Δ_{H3}, and Δ_{H4}: the corresponding slip of the fiber when pullout load reaches P'_{H1}, P'_{H2}, P'_{H3}, and P'_{H4}, respectively; P'_{C1}: the pullout load when the fiber is completely debonded; P'_{C2}, P'_{C3}, P'_{C4}, and P'_{C5}: the pullout load of 3, 2, 1, and 0 plastic hinge(s) under deformation, respectively; Δ_{C1}, Δ_{C2}, Δ_{C3}, Δ_{C4}, and Δ_{C5}: the corresponding slip of the fiber when pullout load reaches P'_{C1}, P'_{C2}, P'_{C3}, P'_{C4}, and P'_{C5}, respectively.

matrix of UHPC, a gradually decreasing load (P'_{S2}–P'_{S3}) shows the fiber debonding [46]; in case of normal concrete, the load decreases rapidly. After complete debonding, sliding friction governs the nonlinear pullout response. The fiber–matrix contact area is reduced as the slippage develops, resulting in decreased pullout load between the straight fiber and matrix. The post-cracking stage exhibits a random pullout force–slippage relation because of the frictional fiber–matrix interfacial bond. The pullout load declines after reaching the peak. Finally, pullout failure occurs when the fiber is completely detached from the matrix [41].

(2) **Hooked-end fiber.** Fig. 6(b) shows that the pullout behavior of a hooked-end fiber consists of five stages [53]: ① elastic and partial debonding (O–P'_{H1}); ② strain hardening (P'_{H1}–P'_{H2}); ③ stress relaxation (P'_{H2}–P'_{H3}); ④ second plastic deformation (P'_{H3}–P'_{H4}); ⑤ straight pullout (P'_{H4}–S'). P'_{H1} is the pullout load when the fiber is completely debonded. P'_{H2} is the first plateau load due to the contribution of two plastic hinges. P'_{H3} is the second plateau load when only one plastic hinge works in matrix. P'_{H4} is the pullout load without plastic hinge. Δ_{H1}, Δ_{H2}, Δ_{H3}, and Δ_{H4} are the corresponding slip of the fiber when pullout load reaches P'_{H1}, P'_{H2}, P'_{H3}, and P'_{H4}, respectively.

At stage ①, elastic deformation followed by the debonding of the straight part of the hooked fiber is observed. The mechanism of hooked fiber at stage ① (O–P'_{H1}) is similar to those of stages ① and ② (O–P'_{S2}) for straight fibers. When the pullout load reaches point P'_{H1}, debonding begins, and the fiber–matrix adhesion gradually decreases. After the point P'_{H1}, the slope of the curve becomes

less steep. At stage ② (P'_{H1}–P'_{H2}), mechanical anchorage improves the pullout strength and leads to a slip-hardening behavior. The fiber hook end straightens in the two inflection points of the matrix channel and experiences large plastic deformation, leading to a significant increase in the pullout load until the peak. When the pullout load reaches point P'_{H2}, debonding becomes maximum, and the fiber–matrix adhesion is lost. At stage ③ (P'_{H2}–P'_{H3}), as one hook of the fiber is straightened, the load rapidly falls to the point P'_{H3}. At stage ④ (P'_{H3}–P'_{H4}), after a slip-softening behavior of fiber, pullout load slightly increases or remains stable. Alwan et al. [51] indicated that this slight increase could be attributed to the bending of the fiber in the opposite direction, which causes more anchorage resistance. Then the remaining hook undergoes plastic deformation. At stage ⑤ (P'_{H4}–S'), the fiber is only resisted by the sliding friction and eventually pulled out; this remaining friction is always higher than that for a straight fiber because of the improved surface roughness of the incomplete straightened end hook [54]. When the straightened hook end is pulled out entirely, the pullout load rapidly drops to zero.

For a hooked-end fiber, the mechanical anchorage is generated by the plastic bending of the two ends. Anchorage influences bond behaviors significantly and contributes more to fiber pullout load than adhesion and friction [32]. Generally, debonding is completed at the fiber slip less than 0.1 mm, with less than 1% pullout energy contributed. Hence, the contribution of chemical/physical adhesion can be neglected. During the first fiber slip-hardening stage, the small kinetic friction of the fiber is ignorable until the fiber end

fully enters the straight channel in the matrix at stage ⑤. Due to the anchorage of a deformed fiber, the pullout load nonlinearly increases. Then, this load decreases after reaching the maximum; however, the plateau of the curve remains flat and even goes up at stage ④. A residual load may increase when the fiber end is completely pulled out of the tunnel. In addition, some cases exist in which fiber ends might not be fully straightened and removed a portion of the matrix when it was pulled out [15].

(3) **Corrugated fiber.** The overall pullout process of corrugated fibers has been described in several studies [1,55,56]. Zīle and Zīle [55] considered hooked-end fiber as a special case of crimped fiber, where the geometry of the hook was composed of only two curved segments of length $\rho\theta$ and two straight segments of lengths l_e and l. ρ is the curvature of curved duct, θ is an angle of curved duct wrap, l_e is the length of straight duct at the fiber end, and l is the length of straight duct of the fiber midsection. As shown in Fig. 6(c), fiber segments in curved ducts CD1 and CD2 are subjected to plastic bending and friction, similar to hook segments of hooked-end fiber. Fiber segments in straight ducts SD1, SD2, and SD3 are subjected to frictional sliding.

As shown in Fig. 6(c), the six pullout stages of crimped fiber can be described as follows: ① elastic and debonding (O–P'_{C1}) and ② slip-hardening (P'_{C1}–P'_{C2}), similar to the stages ① and ② in the pullout process of hooked-end fibers. At stage ③ (P'_{C2}–P'_{C3}), the length of the fiber segment in CD1 decreases, resulting in a decreased pullout load caused by mechanical deformation. Fiber segments in CD2 and CD3 still experience bending deformation. Fiber segments in SD2 and SD3 are resisted by sliding friction. At stage ⑤ (P'_{C3}–P'_{C4}), the length of the fiber segment in CD2 decreases. At stage ⑤ (P'_{C4}–P'_{C5}), fiber is pulled out through SD3 and CD3, which leads to complete loss of mechanical anchorage.

Finally, at stage ⑥ (P'_{C5}–S'), only frictional sliding exists in SD4. P'_{C1} is the pullout load when the fiber is completely debonded. P'_{C2}, P'_{C3}, P'_{C4}, and P'_{C5} represent the pullout load of 3, 2, 1, and 0 plastic hinge under deformation, respectively. Δ_{C1}, Δ_{C2}, Δ_{C3}, Δ_{C4}, and Δ_{C5} are the corresponding slip of the fiber when pullout load reaches P'_{C1}, P'_{C2}, P'_{C3}, P'_{C4}, and P'_{C5}, respectively.

(4) **Comparison of bond behaviors in normal concrete and in UHPC.** UHPC is characterized by a compressive strength of over 120 MPa [57] and generally exhibits excellent bond properties in comparison with normal concrete. Cao and Yu [15] indicated that a sudden sharp drop after the peak load in normal concrete was not observed in UHPC due to the dense microstructure of UHPC, as shown in Fig. 7 [35,58].

For UHPC, a slip-hardening behavior of brass-coated straight fibers, governed by friction, improves the bond toughness after debonding, different from the slip-softening behavior in normal concrete. Extensive surface scratching, as shown in Fig. 8(a) [41], which can be caused by micro sand particles in UHPC matrix [59] or fiber surface treatment applied perpendicularly to the fiber axis [60], may result in a slip-hardening behavior of straight fibers. The abraded surface of fiber provides additional resistance due to kinetic friction. In addition, the slip-hardening behavior in UHPC can also be attributed to the local matrix destruction in pullout behavior when the bond is significantly stronger than the weak ITZ or matrix [61]. As depicted in Fig. 8(b) [62], fiber is pulled out surrounded by a mass of damaged matrix [41]. On the surface of the matrix attached to the fiber, several micro-cracks can be observed. Thus, the channel where the fiber is pulled out is blocked, and the surface becomes rougher. The coefficient of kinetic friction between fiber and matrix and sliding friction is increased. The surface abrasion of fiber and the jamming effect of the matrix can work simultaneously. This slip-hardening behavior is more evident for highly deformed fiber, such as twisted fiber [59], over the entire fiber length because of the strong friction and mechanical force in the entire pullout process.

In addition to the increasing sliding friction arising from fiber scratch and matrix jamming during the pullout process, fiber rupture can occur when the fiber is pulled out from the UHPC. In contrast, the fiber embedded in normal concrete can be completely pulled out, even without being fully straightened. Therefore, instead of only considering the peak pullout stress, the complete stress–slip curve should be considered for UHPC.

3.2.2. Fiber rupture failure mode

Fiber rupture, as a mode of brittle failure, occurs instantaneously, as shown in Fig. 9. This is unfavorable for structural safety. Fiber rupture can occur during the pullout process, typically characterized by a sudden drop appearing before and after the peak slip. Fiber rupture is uncommon in normal concrete due to the weak bond strength between fiber and normal concrete matrix. When the fiber–matrix bond in UHPC is significantly strong, fiber rupture may occur even before the commencement of the potential
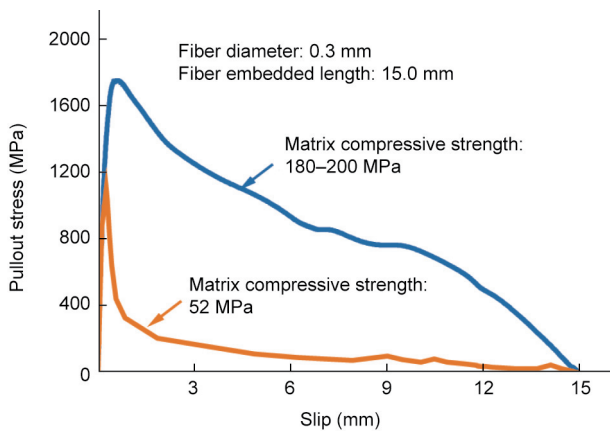
Fig. 7. Pullout stress versus slip of straight fibers in normal concrete (compressive strength of matrix: 52 MPa) [58] and UHPC (compressive strength of matrix: 180–200 MPa) [35].

Fiber diameter: 0.3 mm
Fiber embedded length: 15.0 mm
Matrix compressive strength: 180–200 MPa
Matrix compressive strength: 52 MPa

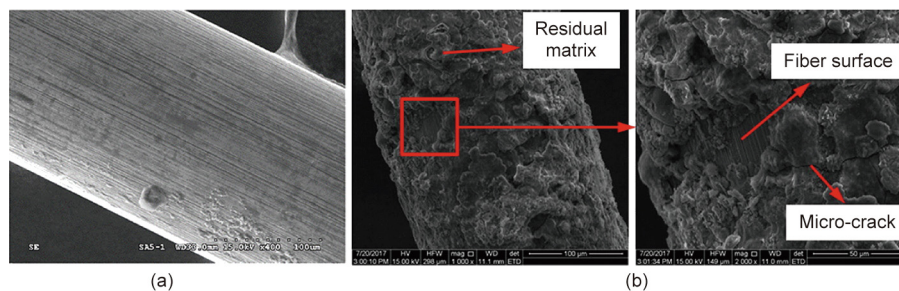**Fig. 8.** Surface microstructure of steel fibers after pullout: (a) surface scratching [41]; (b) residual matrix adhered to the surface [62].

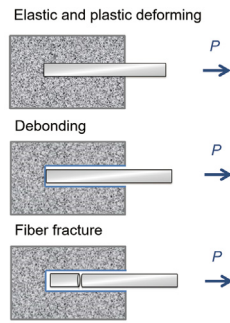Residual matrix
Fiber surface
Micro-crack

Fig. 9. Illustration of fiber fracture process.

fibers function to enhance strength [63]. In summary, when the product of the shearing and surface stresses along the length of the fiber is greater than the product of the cross-section of the fiber and tensile stress on it, fiber rupture will occur. The large aspect ratio, low tensile strength, and high deformation degree of fiber and dense ITZ are the most significant factors in generating the rupture failure mode of steel fiber. A strong ITZ around the fiber enhances fiber–matrix adhesion and friction. Fiber rupture was observed for the hooked fiber with a small diameter of 0.2 mm and an embedded length of 6.5 mm in the matrix of 194 MPa compressive strength [59]. When the diameter of fiber is relatively small or mechanical anchorage of fiber is strong with several hooked ends or bends, the load sharply drops after the fiber fracture [15]. This failure mode may occur at any portion of the hook [63]. In comparison, less deformed fibers in the relatively low-strength matrix were completely pulled out. Fiber tension failure was observed in the case of hooked-end fiber and twisted fiber with large inclination angles and possibly high loading rates [14].

4. Theoretical models

Theoretical models are essential for the prediction of pullout behavior, eliminating the need for bond experiments. To date, very few pullout models have been specifically developed for the assessment of steel fiber embedded in UHPC. Currently, the models of fiber-reinforced concrete are adopted for UHPC. The well-known fiber pullout models for straight and deformed fibers are specified in this section. Most of the proposed models describe the bond behavior between fiber and plain matrix [37]. As hybrid fibers are significantly beneficial in enhancing the bond properties, a pullout model considering multiple-type fibers needs to be investigated in the future.

4.1. Straight fiber

Various theoretical models have been proposed to simulate interactions between straight fiber and concrete matrix. The basic shear-lag model was proposed to represent the fiber–matrix tensile stress [64]. The simplest model was a straight fiber in a cylindrical matrix [65], where the fiber was assumed to be bonded rigidly and transfer insignificant tension in a homogeneous matrix [66,67]. The modeling results were in good agreement with test results for the short embedded fiber in plastic matrix type resin. However, the weak bond between steel fiber and concrete matrix may lead to damage when the matrix is elastic; therefore, the simulation value will be higher than the actual value. Assuming that the elastic shear stress at the interface is related to the relative displacement, Rosen [68], Lawrence [69], and Wang et al. [70] have proposed some developments based on the shear-lag model. In particular, Lawrence [66] proposed a theory of gradual debonding of fiber considering the elastic and frictional shear stress at the interface, where interface debonding initially occurs near the extraction point and then develops in depth along the interface.

Naaman et al. [71,72] expressed the bond shear stress τ as functions of the fiber slip s, as shown in Fig. 10 [72]. The effects of fiber shrinkage after debonding, static friction, and kinetic friction were considered in this model. According to this model, in the elastic bond stage, the shear stress–slip relationship is linear with a constant gradient k related to static friction. After the maximum shear stress, complete debonding is achieved, followed by the sliding friction stage. When the fiber is pulled from the axial direction, it will shrink in a radial direction, which will weaken the frictional shear stress τ_f. Thus, in order to conform to the actual situation, they expressed the descending segment as an exponential function after actual tests [72]. However, the model computation is complex, and the chemical adhesion independent from slippage is assumed to be negligible in this slip-induced model. In addition, Lee et al. [26] reported that the sudden drop from the maximum bond strength τ_{max} to the frictional shear stress τ_f, which usually occurs in normal concrete as shown in Fig. 10(a) [72], would not happen in ultra-high strength mortar (UHSM). Fiber debonding starts in UHPC when τ_{max} is equal to τ_f, as shown in Fig. 10(b) [72]. The difference between the pullout models is associated with the high friction in the fiber debonding section in UHPC. The debonding mode can be explained by comparing the maximum shear strength and the shear strength when debonding starts or fracture mechanics [73]. The applicability of shear strength or fracture mechanics theories changes with the material, volume ratio, diameter, and embedded length of fiber and the matrix material [74,75]. Lee et al. [26] also proposed a semi-empirical model for decaying friction suitable for UHPC and suggested that the actual
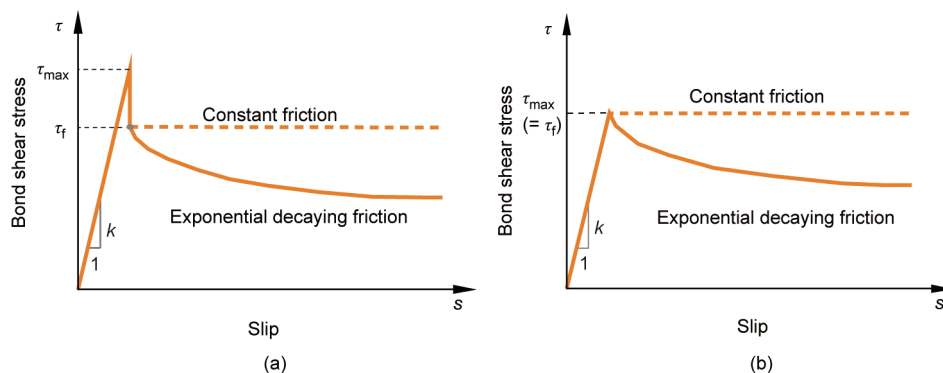

Fig. 10. Relationships between bond shear stress τ and fiber slip s for straight fiber: (a) $\tau_{max} > \tau_f$; (b) $\tau_{max} = \tau_f$ [72]. The gradient k in the elastic stage is a constant. τ_{max} is the maximum bond strength and τ_f is the frictional shear stress.

decay of the frictional bond stress in UHSM, and particularly in UHPC, should be adjusted according to matrix characteristics. Furthermore, for inclined fiber in UHPC, elastic deformation of the fiber, snubbing effect, and matrix spalling were considered; nevertheless, the possible slip-hardening behavior was not considered when the frictional stress–slip relation of UHPC was proposed.

Zhan and Meschke [76] proposed an interface law model of straight fiber considering the shear-lag theory. According to this model, the maximum bond strength τ_{max} is equal to the frictional shear stress τ_f and remains constant from debonding start point (s_0) to completion point (s_1), as shown in Fig. 11. The controlling point (s_{ref}) for the descending curve is reached when the shear stress decreases to the asymptotic value of the frictional stress τ_{min}. In comparison with Naaman's model, this τ–s relation is relatively simple and has been applied in a few studies [17,41]. Considering the aging effect on load–slip relationship by changing the interfacial pressure, Zhang et al. [17] revised the model of Zhan and Meschke [76]; the improved model was able to predict the bond strengths at 3, 7, 28, and 91 days.

4.2. Deformed fibers

The entire pullout process curve for deformed fibers is significantly more complicated than those of straight round fibers because of the complex pullout failure models. Interface mechanisms of fibers with different geometries are different. Hooked-end fibers were applied earlier than other deformed fibers; therefore, several models have been developed for hooked-end fibers. In addition, some analytical models exist to simulate the pullout process of a pre-deformed fiber based on virtual work (energy conservation), fracture mechanics, and empirical analyses [61].

Based on the balance of mechanical energy, Chanvillard [77] proposed a model considering the effects of mechanical deformation, cohesion, and friction. In this model, one fiber is divided into small elements with a specified curvature along the axial direction. Then the parameters of the model are numerically integrated and superimposed to fitting the loading–slip curve. This model was applied by Chanvillard to study the behavior of straight, semicircular, hooked-end, and corrugated fibers; however, the local crushing effect, which could be introduced by the proportional embedded fiber length during the pullout process, was not considered in this model [20]. Furthermore, the transfer of bending moment and shear force between microelements and the changes in interface pressure caused by them were neglected in the analysis model. The balance of the mechanical energies can be expressed as Eqs. (12)–(14):

$$W_{ext} = W_{def} \tag{12}$$

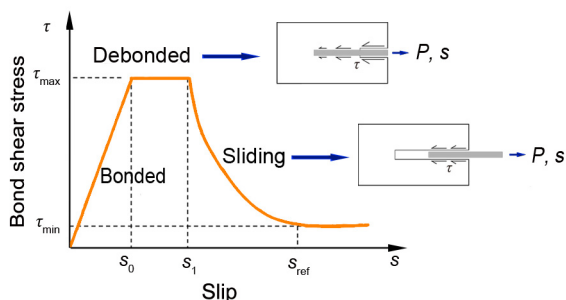$$W_{ext} = dP \cdot d\delta \; - \; dT \cdot d\delta \tag{13}$$

Fig. 11. Relationship between straight fiber bond shear stress versus slip considering debonding in the model [76]. τ_{min}: the asymptotic value of the frictional stress; s_{ref}: the controlling point for the descending curve.

$$W_{def} = dC \cdot ds_c \int_{S_c} z \cdot \sigma_\varepsilon \cdot dS \tag{14}$$

where W_{ext} is the work done by the pullout load; W_{def} is the deformation energy; δ is the rigid body displacement; dT is the tangential component; dC is the curvature variation; s_c and z is the curvilinear coordinate, and radial coordinate, respectively; σ_ε is the stress governed by the strain state; and S is the surface of the fiber section.

Alwan et al. [51] proposed a frictional pulley model for the hooked-end fiber based on the pullout model of smooth fibers—a model originally developed by Naaman et al. [71]. This model assumes that the bending point of the fiber forms a plastic skein during the process of anti-pullout. The model considers this as a "pulley" to analyze the mechanical deformation, as shown in Fig. 12(a) [51,53], based on static force and moment equilibrium during the pullout of the deformed fiber. In Alwan's frictional pulley model, the hooked-end fiber is pulled out, as shown in Fig. 12(a) [51,53], where F, F_{PH}, T, β, and R are the tangential friction component, rotational friction component calculated by the work required to straighten the steel fiber at the plastic hinge, chord tension, hook angle and reaction force at the pulley center. The pullout process is divided into four stages according to the positions of the sections of plastic hinges. The pullout load, P, of each stage, is the summation of forces on the straight and hook parts. However, the axial action of fiber is assumed to primarily provide a bending moment instead of the interface action in the model. Further, the higher sliding friction of the straightened hook, arising from the uneven surface of the straightened segment, should be separated from the friction of the smooth fiber segment, as proposed by Deng et al. [40]. In addition, when the displacement reaches Δ_4, as shown in Fig. 12(a) [51,53], a sudden load drop related to the complete straightening of the hook end is neglected. Moreover, considering the actual situation, the curve can be a second-degree polynomial (parabola) with the peak P_2, the pullout load during the first plateau, as the slip changes from Δ_1 to Δ_3.

The force P_{cr} represents the critical load which triggers debonding. The force P_1 can be obtained using Naaman's model for the straight fiber, while P_2, P_3, and P_4 are calculated using Eqs. (15) and (16):

$$P_2 = P_3 = P_1 + \Delta P' \tag{15}$$

$$P_4 = P_1 + \Delta P'' \tag{16}$$

where P_1, P_2, P_3, P_4, $\Delta P'$, and $\Delta P''$ are the pullout loads at onset of complete debonding, during mechanical interlock with all plastic hinges, during the plastic hinge is reduced by one, during the plastic hinge is reduced by two, contributed from two plastic hinges, and contributed from one plastic hinge, respectively.

In recent studies, several analysis models have been proposed. Some models were developed based on the virtual work theory of Chanvillard. For instance, Soetens et al. [78] proposed a semi-analytical model to simulate and predict the pullout curves of inclined hooked steel fibers embedded in the matrix of various compressive strengths. Similarly, Feng et al. [61] developed a model for hooked-end fiber in UHPC based on Naaman's model of straight fiber. This model showed higher peak-matching accuracy than that of the previous models for fiber with different embedded lengths [55,79]. In particular, to consider the matrix spalling at the fiber exit, it was assumed that the bond shear stress did not act on the hooked parts. Furthermore, slip-hardening caused by the abrasion and jamming effect was incorporated through the introduction of the spalling length, together with additional friction due to bending and Coulomb friction. However, the effect of cracked matrix attached to the end hook was neglected in correlation with the slight increase in friction resistance when fiber end was pulled out.
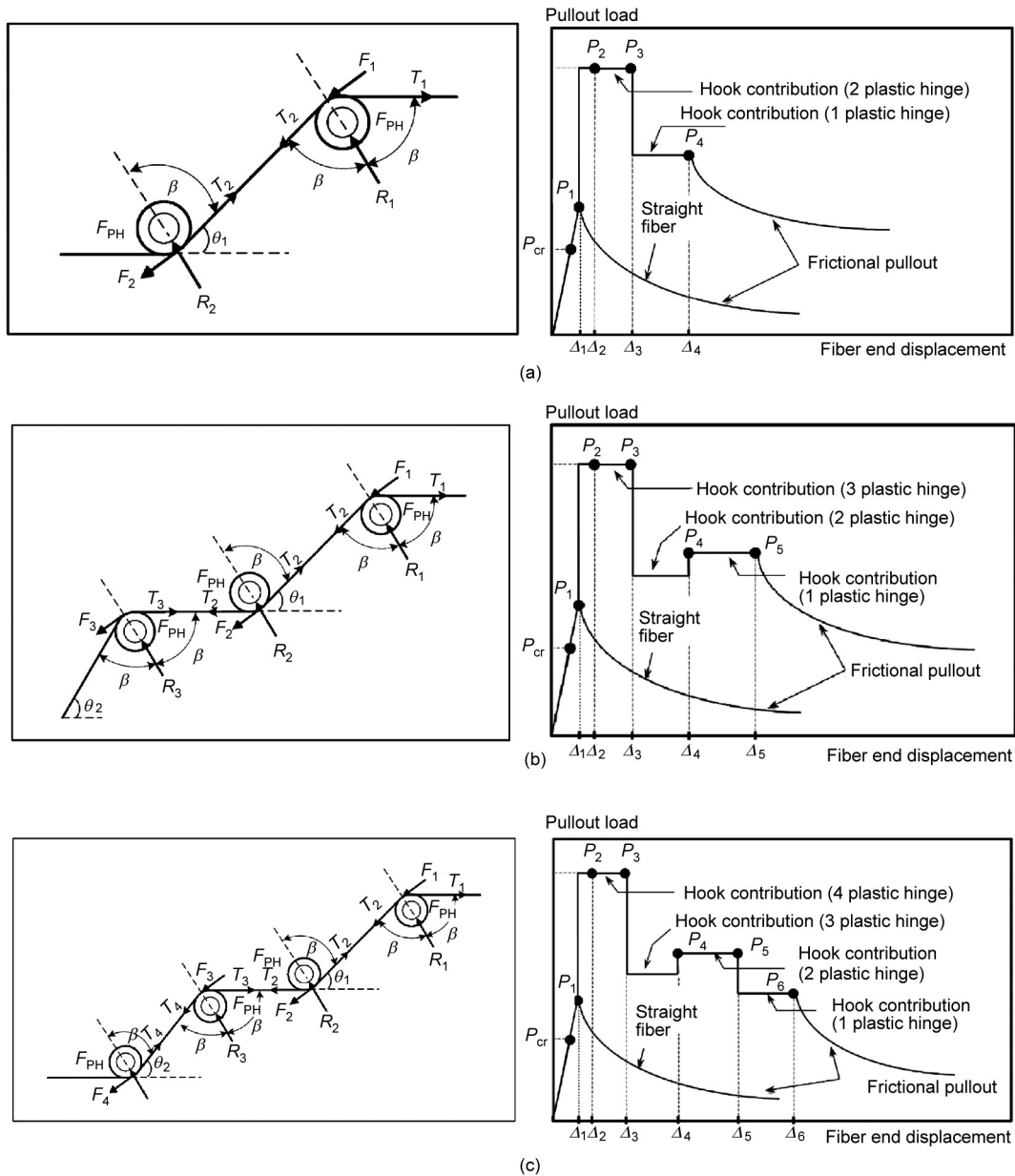
Fig. 12. Line sketches of the frictional pulley models of Dramix hooked fibers with (a) three segments (3DH), (b) four segments (4DH), and (c) five segments (5DH) and their corresponding theoretical pullout curves [51,53]. θ_1 and θ_2 are hook angles; F: the tangential friction component; F_{PH}: the rotational friction component calculated by the work required to straighten the steel fiber at the plastic hinge; T: the chord tension; β: the hook angle; R: the reaction force at the pulley center; P_{cr}: the critical load which triggers debonding; P_1, P_2, P_3, P_4, P_5, and P_6: the pullout loads at onset of complete debonding, during mechanical interlock with all plastic hinges, during the plastic hinge is reduced by one, during the plastic hinge is reduced by two, during the plastic hinge is reduced by three, during the plastic hinge is reduced by four, respectively; Δ_1, Δ_2, Δ_3, Δ_4, Δ_5, and Δ_6: the corresponding fiber end displacements when pullout load reaches P_1, P_2, P_3, P_4, P_5, and P_6, respectively.

Other existing models are based on the frictional pulley model of Alwan. For instance, Abdallah et al. [53] and Abdallah and Rees [80] extended the work to various hooked fibers with multiple deformed segments in ultra-high strength matrix. The extended model, as shown in Figs. 12(b) and (c) [53], was based on the frictional pulley model of Alwan. In this model, the fiber rupture condition was considered by comparing the fiber ultimate strength and the peak bond stress, as the completely straightened fiber is possible to be over utilized in UHPC. The uncomplete straightening of fiber was discussed by combining the elastic–plastic moment expression in Ref. [80]. However, the aforementioned shortcomings of the frictional pulley model still existed in Abdallah's model. Moreover, the elastic and debonding stages of the multiple bending segments of hooked fiber was neglected in this model, though which is acceptable for normal hooked fiber with a short end. Fur-

thermore, the model ignored the local damage in the matrix around the hook.

In addition to the models related to Chanvillard's or Alwan's models, some independent analytical models for deformed fibers exist. These models, primarily applied to normal concrete, can assist in understanding bond behaviors of various deformed fibers in UHPC in the future. Sujivorakul et al. [81] presented a time-consuming model, in which the effect of mechanical resistance of fiber hook was considering using a nonlinear spring. Ghoddousi et al. [82] presented a model for hooked fiber without considering any previous model. In some cases, the results of the model did not match with the actual experimental curves when the spalling of matrix and effect of incomplete straightening of fiber were ignored. They calculated the plastic bending of the fiber and sliding friction in curved and straight ducts, respectively. The elastic

strains and matrix damage were neglected. Assuming straight and curved segments in the fiber geometry, Zīle and Zīle [55] simulated the mechanical contribution when a hooked or crimped fiber was pulled out. Won et al. [83] investigated the pullout behavior model of arch-type fiber based on Zīle's model.

5. Parameters affecting fiber–matrix bond

The fiber–matrix bond behavior of UHPC depends on the characteristics of fiber, matrix, and their interaction [61]. Some recommendations on mixture design of UHPC and related mechanisms are summarized in Table 3 [22,23,32,37,46,59,60,63,84–86]. Generally, surface treatment and orientation of fiber and matrix packing density affect physicochemical adhesion and friction. The fiber geometry influences the mechanical bond via the fiber anchorage.

5.1. Geometry of fiber and surface treatment

Discontinuous short steel fibers, commonly used in UHPC, are shown in Fig. 13 [13]; they are classified into as fibers with and without mechanical bonds [59]. Mechanical anchorage can significantly improve bond properties; therefore, deformed fibers are preferred to straight and smooth fibers [87].

The fiber surface treatment (oiled, coated by brass and zinc, or soaked in chemical solution) and etched or roughened surface can increase the physicochemical bond along with the fiber. The scratched or even completely peeled-off brass fiber coating leads to slip-hardening behavior. Chun et al. [60] observed an increase in the bond strength up to 66% in UHPC when the straight fibers were polished using sandpapers parallel to the fiber axis; a slip-hardening behavior was observed when the surface treatment was applied perpendicularly. The perpendicular sanding direction and the large sandpaper roughness resulted in enhanced bond properties and high lateral pressure by limiting the movement of the abrasion byproducts and increasing fiber surface roughness. Surface corrosion of steel fiber can also change fiber–matrix bond properties in UHPC, which arises from the substantial early-age shrinkage. Yoo et al. [18] investigated the bond behavior of straight steel fibers after immersing these in the 3.5% NaCl solution; when the corrosion degree changed from 0 to 5%, the average bond strength and pullout energy of the fiber attached to the rust layer increased from 6.9 to 14.1 MPa and 390 to 716 mJ, respectively. The rougher fiber surface enhanced the bond properties as a result of the corrosion [48] until the fiber ruptured due to the reduced fiber cross-section. The fiber rupture can cause sudden tensile failure of UHPC, therefore 2% corrosion degree was considered as an upper limit.

Pre-deformed fibers can be divided as follows: fibers with end deformation, such as paddles, buttons, or hooks; fibers with deformations along the fiber, such as crimped, indented, or polygonal twisted fibers [7]. The fiber end bending can increase matrix stress concentration, while the deformation along the fiber, such as the torsion, reduces stress concentration in the matrix. The pullout behaviors of straight, hooked, half-hooked, and twisted fibers are compared in Fig. 14 [37]. Hooked-end fiber is the most extensively studied among deformed fibers. The fiber end bending causes mechanical anchorage and additional friction by inducing pressure in the matrix. Abdallah and Fan [63] discussed the effect of the bending degree of DH steel fibers in UHPC. The maximum pullout load of 5DH (triple bends) and 4DH (double bends) fibers were 63% and 29% higher than that of 3DH (single bend) fibers, and the total pullout work was 27% and 11% higher than that of the 3DH (one bend) fibers, respectively. Zhang et al. [84] observed that the pullout resistance and pullout energy of the more corrugated fiber was increased significantly compared to the less corrugated and hooked fibers; however, the pullout resistance of the double hooked-end fiber was not improved compared with the single hooked one, suggesting further investigation is needed. Yoo et al. [37] investigated the effects of hook length and three different end-hook angles (30°, 45°, and 60°) of fiber on the bond behavior in UHPC. Increasing the end-hook length from 2.5 to 5.0 mm enhanced the static bond strength by 70% because of the increased mechanical deformation during pullout. However, the average bond strength was slightly enhanced with an increasing end-hook angle because the higher stress concentration counterbalanced the positive effect of the larger end-hook angle on the bond strength. Wille and Naaman [59] reported that the bond of twisted fibers was 4.7 times stronger than that of smooth fibers. Twisted fibers also showed more evident slippage-hardening behavior than hooked-end fibers. Some researchers also investigated the bond properties of half-hooked, twisted, round-crimped, arch-type, and flattened-end fibers in UHPC [19,37,49,62,88–91]. The flat-crimped and double-anchored fibers have been investigated only in normal concrete [92]. Deformed fibers generally show high material utilization from 90% to 100%, more than twice the value of straight fibers. However, Park et al. [35] reported the failure of deformed fibers with an embedment length of 15 mm, indicating that high material utilization decreases the ultimate fiber tensile strength and increases the risk of fiber rupture.

In conclusion, for straight fibers, the pullout properties are predominantly governed by physicochemical and frictional bonds, which are affected by surface treatment and matrix density. For deformed fibers, these properties are dominated by mechanical

Table 3
Mechanisms and mixture design for improving bond properties in UHPC.

| Mechanism	Recommendations on mixture design	Refs.
Increased surface roughness of fiber	Use fiber with polished surface	[60]
Increased mechanical deformation of fiber	Use highly deformed fibers with high tensile strength: multiple bends at hook end, long hook end, highly twisted and highly corrugated fibers	[59,63,84,85]
Orientation of fiber	Use straight and half-hooked fibers instead of hooked or twisted fibers for increasing bond properties at random inclination angles	[37]
Enhanced matrix density		
Congestion of hydration products at interface	Use a w/b ratio lower than 0.2	[32]
Addition of pozzolanic reactive material	Use 15%–25% silica fume (by the total mass of binder)	[22]
Addition of nano-materials associated with filling and nucleation effects	Use approximately 1.0% nano-SiO$_2$ or 3.2% nano-CaCO$_3$. The optimal content changes depending on mixture composition, water dosage, and flowability requirement	[23,46]
Enhanced particle dispersion	Adopt two types of fine sand with various grain sizes in a proper proportion, low sand-to-cement ratio, and very fine glass powder	[59]
Inhibition of crack development on micro- and macro-scales	Use hybrid steel fibers	[86]
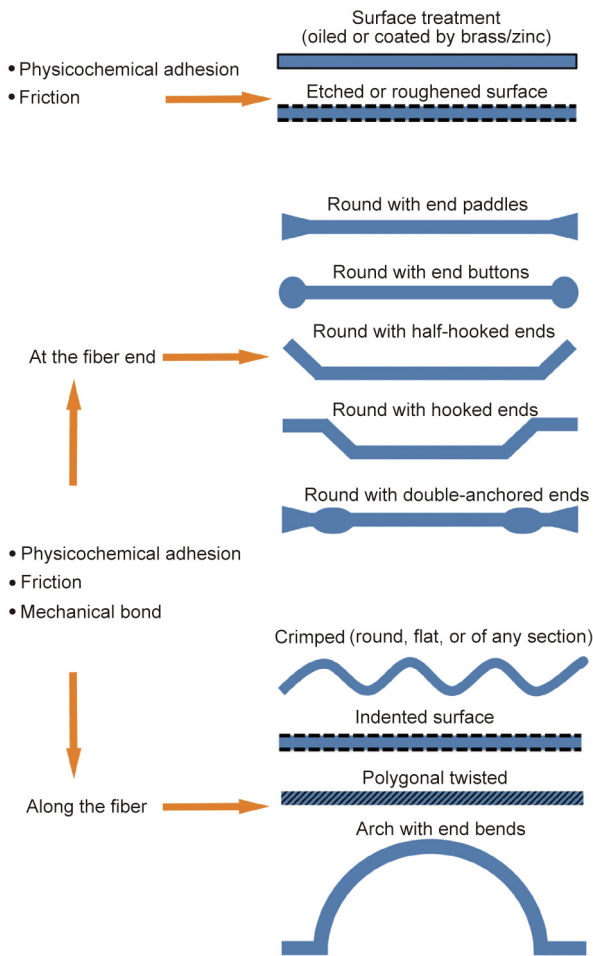
Fig. 13. Classification of steel fibers and their pullout mechanisms [13].
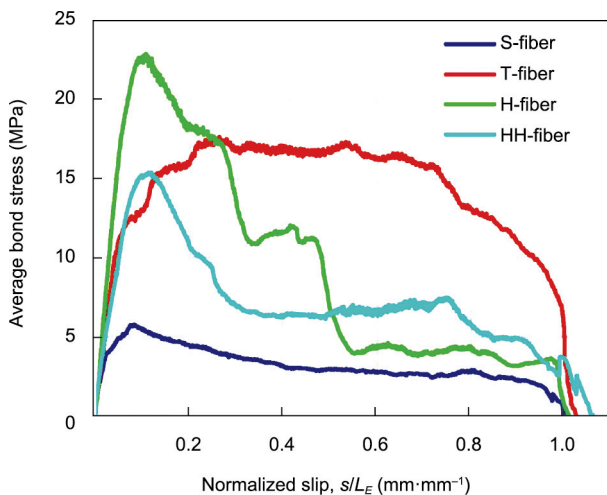

Fig. 14. Pullout behaviors of straight (S), twisted (T), hooked (H), and half-hooked (HH) steel fibers in UHPC matrix [37].

bonds; these fibers can enhance the bond performances by three to seven times compared to straight steel fibers [19] but at an increased risk of fiber breakage. Thus, highly deformed fibers with high tensile strength can be adopted to enhance bond properties in UHPC. However, utilizing surface-treated straight fiber is more feasible for obtaining stress hardening behavior.

5.2. Orientation of fiber

The fiber orientation is not always perpendicular but oblique to the cracking surface because of the random distribution of short fibers in the matrix [93]. However, the random distribution hypothesis of fibers might not be accurate and realistic due to the matrix edge effect. Consequently, the axial pullout model cannot completely reflect the crack-bridging mechanism of fiber in composites after cracking [94]. Debonding, deformation, and sliding behaviors occur when the fiber is pulled out vertically. However, the bending, tensile, rupture, and yield failure of fiber, and the partial yield, rupture, and spalling of matrix could also be observed in real situations, which introduces numerous complex changes to the analysis of the problem.

A favorable orientation of fibers may cause high pullout resistance within a certain range. Yoo et al. [37] demonstrated that the highest pullout resistances of straight, hooked, half-hooked, and twisted fibers were obtained at an inclination angle between 30°–45°, instead of 0° or 60°, as shown in Fig. 15(a). They also reported that slip increased with an angle, as shown in Fig. 15(b) [37]. The increased slip might be attributed to severe matrix spalling, which decreased the embedded fiber length. The sudden decrease in slip for hooked fiber at 45° was related to fiber rupture. In Fig. 15(c) [37], the trend of fiber tensile stress was similar to that of the peak average bond strength. Considering the fiber rupture and matrix spalling effects according to inclination angle, Lee et al. [26] expressed the apparent shear strengths of straight fibers as a function of inclination angle, as shown in Fig. 16. The peak apparent shear strength at 45° implied that the maximum bond occurred at the inclination angle of 45°. Similarly, Qi et al. [41] reported that the average bond strength increased by 19.0% and 52.9% at 30° and 45° for straight fibers, respectively, while 10.3%–13.6% at 30° and 16.2–26.1% at 45° for hooked fibers. Tai and El-Tawil [14] demonstrated that straight, hooked, and twisted fibers reached peak load resistance at 45°, 30°, and 15°, and the peak pullout load increased by 79%, 23%, and 39%, respectively. However, Cao and Yu [15] reported the effect of the orientation angle on the pullout load was insignificant when matrix spalling reduced the embedded length of fiber at 20° and 30° instead of 45° and 60°, as reported in other studies. Similarly, the normalized pullout energy of twisted and hooked fibers decreased significantly when the inclination angle was increased, as shown in Fig. 15(d) [37]. The decreased pullout energy was attributed to the matrix damage during pullout, which was associated with the decreased fiber embedded length. Further, straight and half-hooked fibers effectively enhanced the bond energy compared to hooked and twisted fibers. Therefore, the pullout load–slip model with a fiber inclination angle of 0° could not be directly applied to structural design considering the possible negative effects of fiber inclination on the bond.

The occurrence of fiber rupturing failure and matrix spalling significantly depends on fiber orientation. In general, the fiber fracture strength decreases with the inclination angle caused by the additional shear stress imposed on the fiber. In seven out of ten tests, a hooked-end fiber—diameter of 0.38 mm and embedded length of 10 mm—ruptured under an inclination angle of 30°, due to the strong bond and anchorage of the UHPC matrix [15]. In contrast, a large fiber—diameter of 0.9 mm and embedded length of 15 mm—showed complete pullout behavior and exhibited a better ductile response under inclination angles of 10°, 20°, and 30°. All half-hooked fibers were ruptured at 45° [30]. In ultra-high strength cementitious mortar, it was observed that the decay behavior, due to the frictional slip after the peak load, was independent of the fiber inclination [26].
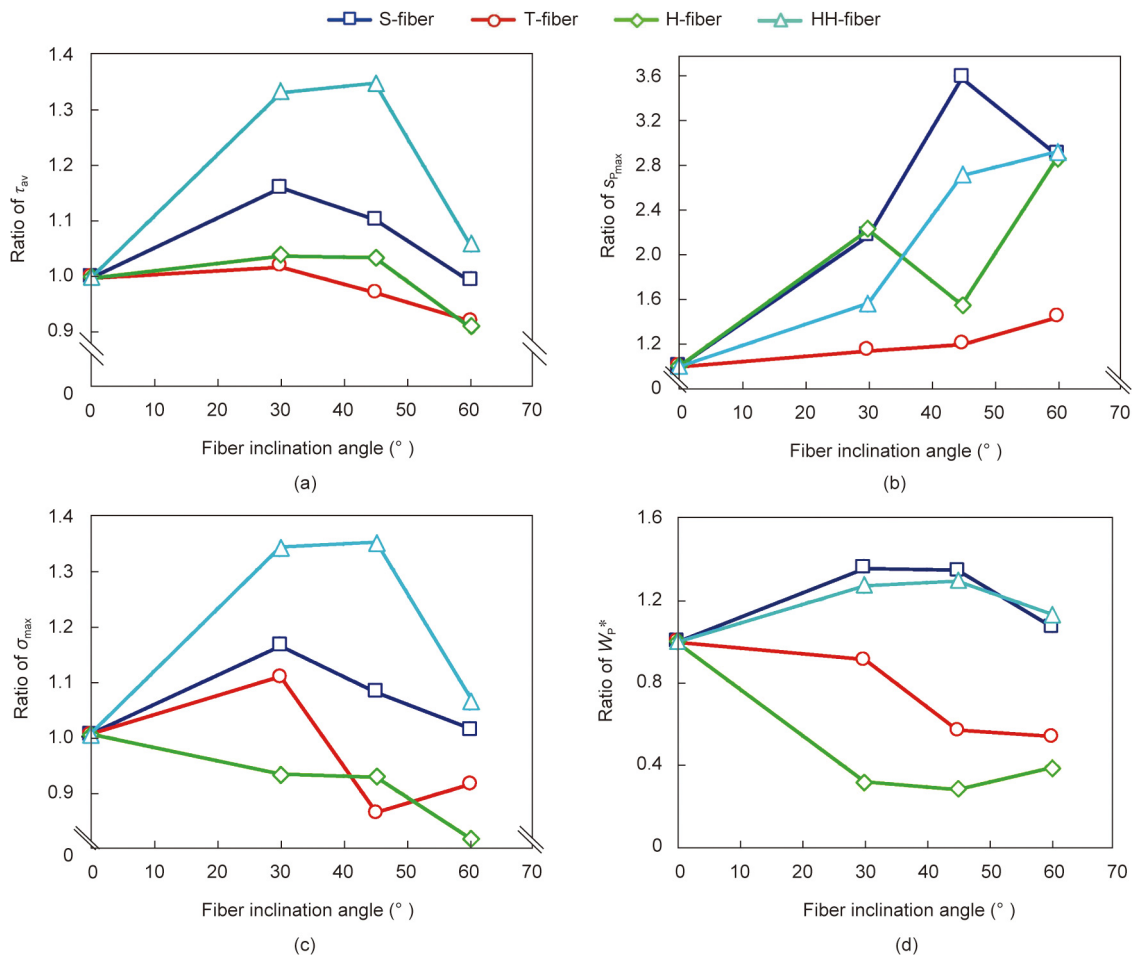
Fig. 15. Effects of inclination angle on normalized pullout ratios of (a) average bond strength, (b) slip capacity, (c) maximum fiber tensile stress, and (d) pullout energy in UHPC matrix [37]. The parameters ratios are based on the aligned fiber specimens at 0° inclination angle. s_{Pmax} is the fiber slip corresponding to the peak pullout load. The normalized pullout work W_P^* can be calculated from the area under the bond stress-normalized slip curve for comparing the steel fibers with different diameters and embedment lengths.
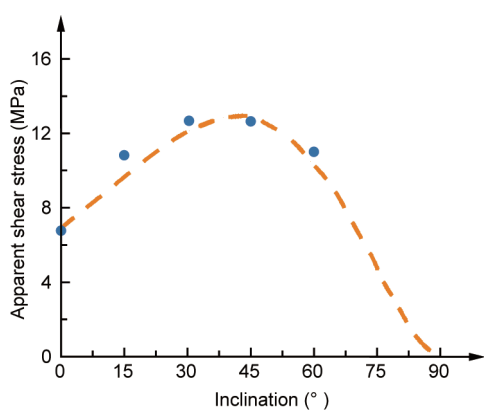

Fig. 16. Apparent bond strength as a function of inclination angle of straight fiber [26].

5.3. Strength and components of matrix

The strength grade is an index of the densification of matrix, which is an inherent factor that affects the bond properties of fiber. The bond properties, particularly the pullout toughness, have a positive relationship with the matrix strength (i.e., compressive strength) [90].

For straight fibers, Yoo et al. [95] reported that an increase in the matrix compressive strength from 112.2 to 190.2 MPa enhanced the average bond strength and pullout energy of straight steel fibers by 1%–20% and 6%–30%, respectively. For deformed fibers, the increase in the bond properties was less than 10% when the compressive strength of matrix increased from 112.2 to 190.2 MPa. Wille and Naaman [20] demonstrated that increasing the matrix strength from 207 to 240 MPa could increase the average bond strength and pullout energy of straight fiber by 100% and 66%, respectively. The bond properties of fiber are more significantly affected by fiber deformation (three to seven times as mentioned in Section 5.1) than the increasing rate of matrix strength of UHPC. Therefore, to improve pullout behavior of fiber in UHPC, it might be more beneficial to change the fiber geometry.

Generally, a high matrix strength does not guarantee a good bond performance. Fiber tensile and matrix strengths should be compatible with each other to obtain the best pullout load economically while fully utilizing the potential of high strength steel fiber. In contrast, when the strength of matrix is low and incompatible with the tensile strength of fiber, the pullout load could be substantially low. Abdallah and Fan [63] observed that mechanical anchorage did not fully contribute to bond behavior in normal and medium strength concrete matrixes, while it was significantly better in UHPC (Fig. 17). Incomplete straightening of deformed fiber constricted by porous normal concrete results in a 'waste' of fiber tensile strength during pullout. When matrix strength is high

and thus the bond strength is stronger than the tensile strength of fiber, fiber breakage occurs. Fiber rupture characterized by a sharp load drop occurred at a small slip in UHPC for 3DH and 4DH fibers, as shown in Figs. 17(a) and (b). Multiple bends at hook end reduced the tensile strength of 3DH (1150 MPa) and 4DH (1500 MPa) fibers [63] and, together with the dense fiber–matrix interface [33], caused fiber fracture. In contrast, sufficiently deformed 5DH fiber with a high fiber tensile strength of 2300 MPa exhibited a good pullout performance, as shown in Fig. 17(c) [63]. Therefore, it is important to adjust the fiber geometry and the fiber tensile strength according to the properties of UHPC matrix to improve bond strength and ductility.

Low w/b ratio in related to high matrix strength leads to high bond strength. Abdallah et al. [32] indicated that the decrease in the w/b ratio from 0.20 to 0.15 influenced significantly on bond behavior compared to that in w/b ratio from 0.25 to 0.20. The maximum pullout load of hooked fiber was improved by approximately 19% and 1%, respectively. These results were consistent with the findings reported by Yoo et al. [95]: The increase in the bond strength of hooked fiber remained less than 5% when the w/b ratio changed from 0.30 to 0.25 and from 0.25 to 0.20. The hydration

products congested the fiber–matrix interface in UHPC with low w/b ratio, leading to enhanced bond properties [33].

The bond properties can be enhanced using mineral admixtures and nano-materials in UHPC. The addition of 15%–25% silica fume by the total mass of binder in UHPC improved the bond strength of straight steel fiber by 170% [22]. The pullout peak load and pullout energy of UHPC increased by 45% and 200%, respectively, when 3.2% nano-$CaCO_3$ was added [23], and 35% and 70%, respectively, with the addition of 1% nano-SiO_2 [46]. Due to the nucleation effect and chemical reaction with cement or hydration products (e.g., pozzolanic effect), the matrix becomes more compacted with reduced porosity when the content of nano-materials increases. However, an excessive amount of silica fume and other superfine (nano-sized) materials can introduce air and cause agglomeration problems, resulting in pores and cracks near the fiber–matrix interface, eventually leading to low bond strength.

The size, type, and packing density of aggregate in the UHPC matrix also affect the bond behavior. For fine aggregates, Wille and Naaman [20] demonstrated that sands of SiO_2 or $ZrSiO_4$ might scratch the fiber surface during pullout, resulting in high sliding frictional bonds; for coarse aggregates, the weak ITZ between the aggregate and matrix may cause cracks and low bond strength. However, appropriate type, size, and amount of course aggregate can be effective in reducing cost and shrinkage [96], thus improving workability and impact load resistance [62] without reducing bond strength in UHPC. The pullout load–slip curve of UHPC containing basalt aggregate of sizes 1–3 mm exhibited good bond strength [15]. Wille and Naaman [60] also reported that fine sand with a granular distribution enhanced fiber–matrix bond properties due to high packing density. Appropriately adjusting the sand-to-cement ratio (from 1.38 to 1.01) and the proportion of small to large grain sand (from 20% to 30%), the peak pullout load can be increased by approximately 100%. The enhanced particle dispersion and packing density leads to slip-hardening behavior due to the abrasion of the matrix and wedge effect. It may be worth investigating the effects of size distribution and course aggregates on the bond and tensile behavior of UHPC in the future.

5.4. Other factors

Fiber hybridization and durability: Hybrid steel fibers have been gaining increasing attention [97,98] instead of single-type steel fibers because hybrid fibers enhances bond properties at multiple scales. The fiber hybridization on different lengths can restrict micro- and macro-cracks at different stages of crack development, as shown in Fig. 18 [99]. The advantages of several short fibers and good toughness of long fibers can be gained using the same fiber volume. Chun and Yoo [86] conducted multiple-fibers pullout tests for UHPC based on one straight steel fiber on a micro-scale and three different steel fibers (straight, hooked, and twisted fibers) on a macro-scale. They observed that the average bond strengths of micro straight fibers were improved by 7.8% and 17.4% when 0.5% micro straight fibers were substituted with macro twisted and hooked fibers, respectively, at the total fiber volume fraction of 2%. Generally, the optimal ratio of micro straight fibers and macro deformed fibers ranges from 1.0 to 1.5, and the most effective geometry of macro deformed fiber differs between different studies. Moreover, the bond strength of pure micro straight fibers was even better than those containing macro straight fibers, indicating that macro straight fibers adversely affect the bond properties.

Temperature is a critical factor that may affect the steel fiber pullout behavior in UHPC. Abdallah et al. [100] conducted pullout tests on straight and hooked steel fibers embedded in UHPC exposed to room (20 °C) and elevated temperatures (100–400 °C). They reported that the pullout load for straight fiber after
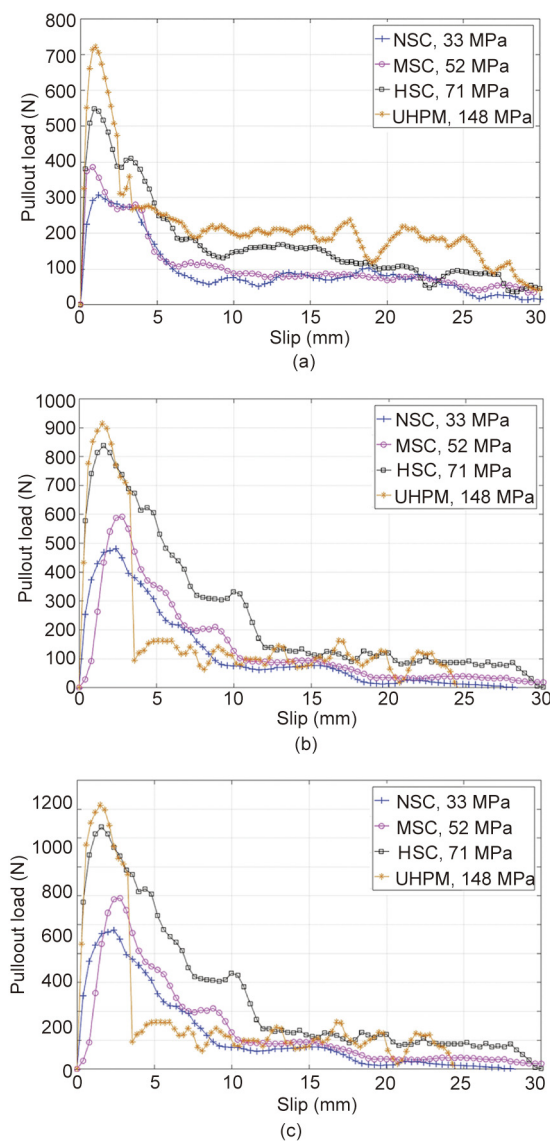

Fig. 17. Pullout behavior of (a) 3DH, (b) 4DH, and (c) 5DH fibers in normal strength concrete (NSC), medium strength concrete (MSC), high strength concrete (HSC), and ultra-high performance mortar (UHPM) matrixes [63].
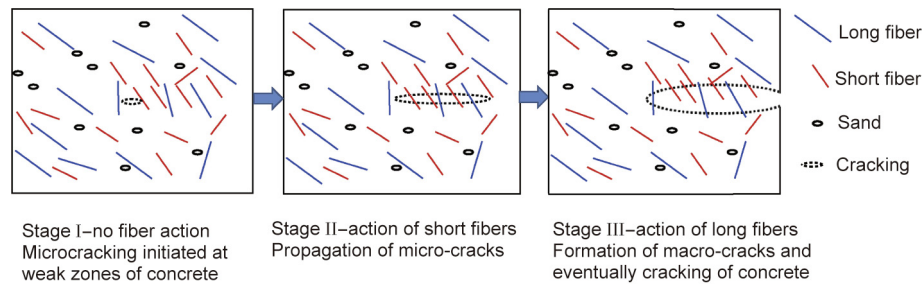
Fig. 18. Crack development in UHPC containing hybrid (short and long) steel fibers [99].

exposure to high temperatures significantly decreased from approximately 299 to 141 N when temperature increased from 20 to 400 °C; this could be due to the significant interfacial damage associated with the low permeability and dense microstructure of UHPC matrix. For the hooked fiber, the equivalent bond strength first slightly increased when the temperature was increased from 20 to 100 °C and decreased with further increase in temperature from 100 to 400 °C. At 400 °C, the compressive strength of the UHPC began to drop, and matrix spalling occurred at temperatures higher than 400 °C. Kim and Yoo [28] observed that the average bond strength increased by 95%, 73%, and 98% for straight, hooked, and twisted fibers, respectively, at a cryogenic (−170 °C) temperature because of higher frictional resistance in UHPC. However, fiber rupture of deformed fibers and extensive matrix damage was caused by stress concentration associated with frozen matrix particles at −170 °C [101]. Therefore, interface change must be considered for mechanical design and application of UHPC under extreme temperature conditions.

6. Conclusions and future research

6.1. Conclusions

From the comprehensive review of the studies on the recent progress of fiber–matrix bonds, several important aspects can be concluded as follows:

(1) Slip-hardening occurs when highly deformed fiber, surface-treated straight fiber, micro sand particles, fiber surface polishing, or chemical solution treatment is applied.

(2) Fiber pullout tests are widely used to evaluate the bond properties between fiber and matrix, among which the multiple-fibers double-sided pullout test is recommended. Future research should focus on the combination of pullout tests with composite theory or macroscopic finite element models. Further, new characterization indexes of the interface bonding performance considering the fiber volume content in the matrix should also be developed.

(3) Physicochemical and frictional bonds govern the bond performance of straight fibers; mechanical bond dominates the bond properties of deformed fibers. In recent years, the use of hooked-end fibers is still higher than other fiber geometries. However, other fiber geometries such as twisted fibers and crimped fibers are receiving increasing attention. The bond performance of deformed fibers can be significantly enhanced by three to seven times compared to that of straight steel fibers. However, the complete stress–slip curve should be studied more extensively.

(4) Increasing fiber inclination angle improves bond performance. However, matrix damage causes a decrease in pullout energy under large fiber inclinations, which can be enhanced by decreasing the aspect ratio of deformed fibers or adopting less deformed fibers.

(5) Matrix strength must synchronize with fiber deformation properly to obtain excellent bond behavior. Adjusting fiber geometry might be more effective than increasing the matrix strength for increasing the bond strength of UHPC. The bond properties can be significantly improved by lowering w/b to less than 0.2, adding pozzolanic reactive material or nano-materials, incorporating SiO_2 or $ZrSiO_4$ sand, and enhancing the particle dispersion.

(6) Potential benefits of hybrid fiber bonds vary with fiber geometry, the ratio of micro to macro fibers, and total fiber volume. The optimal ratio of micro straight to macro deformed fibers ranges from 1.0–1.5 for good bond performance; macro straight fibers always exhibited a negative effect compared to micro straight fibers.

(7) Bond performance of UHPC in terms of durability was investigated. Temperatures above 400 °C impairs bond strength, while the cryogenic temperature (−170 °C) and fiber corrosion can enhance bond properties. Coupling effects of high/low temperature and mechanical load for steel fiber bonds in UHPCs should be considered for future research because actual failure under extreme conditions generally has several coupling factors.

6.2. Future research

Experimental and analytical research related to hybrid fibers is still required. Moreover, to provide a scientific theoretical basis for performance improvement, the modeling of load–slip in UHPC should comprehensively consider the effects of fiber fracture, matrix damage at the anchorage end and along the fiber, compressive strength and age of matrix, slip-hardening, incomplete straightening, and macro-properties of concrete. There is also a requirement for an in-depth and detailed analysis related to bond mechanisms and durability in extreme environments with multiple coupling impacts in order to realize full utilization of the mechanical properties and widespread use of UHPC.

Compliance with ethics guidelines

Yulin Deng, Zuhua Zhang, Caijun Shi, Zemei Wu, and Chaohui Zhang declare that they have no conflict of interest or financial conflicts to disclose.

References

[1] Wu Z, Shi C, He W, Wu L. Effects of steel fiber content and shape on mechanical properties of ultra high performance concrete. Constr Build Mater 2016;103:8–14.

[2] Bajaber MA, Hakeem IY. UHPC evolution, development, and utilization in construction: a review. J Mater Res Technol 2021;10:1058–74.

[3] Ren L, Fang Z, Wang K. Design and behavior of super-long span cable-stayed bridge with CFRP cables and UHPC members. Compos Part B 2019;164:72–81.

[4] Cao YYY, Yu QL, Brouwers HJH, Chen W. Predicting the rate effects on hooked-end fiber pullout performance from ultra-high performance concrete (UHPC). Cement Concr Res 2019;120:164–75.

[5] Wu Z, Shi C, Khayat KH. Investigation of mechanical properties and shrinkage of ultra-high performance concrete: influence of steel fiber content and shape. Compos Part B 2019;174:107021.

[6] Hung CC, Lee HS, Chan SN. Tension-stiffening effect in steel-reinforced UHPC composites: constitutive model and effects of steel fibers, loading patterns, and rebar sizes. Compos Part B 2019;158:269–78.

[7] Naaman AE, Najm H. Bond-slip mechanisms of steel fibers in concrete. ACI Mater J 1991;88(2):135–45.

[8] Gesoglu M, Güneyisi E, Muhyaddin GF, Asaad DS. Strain hardening ultra-high performance fiber reinforced cementitious composites: effect of fiber type and concentration. Compos Part B 2016;103:74–83.

[9] Li PP, Sluijsmans MJC, Brouwers HJH, Yu QL. Functionally graded ultra-high performance cementitious composite with enhanced impact properties. Compos Part B 2020;183:107680.

[10] Feng J, Gao X, Li J, Dong H, Yao W, Wang X, et al. Influence of fiber mixture on impact response of ultra-high-performance hybrid fiber reinforced cementitious composite. Compos Part B 2019;163:487–96.

[11] Su Y, Li J, Wu C, Wu P, Li Z. Influences of nano-particles on dynamic strength of ultra-high performance concrete. Compos Part B 2016;91:595–609.

[12] Ahmad S, Rasul M, Adekunle SK, Al-dulaijan SU, Maslehuddin M, Ali SI. Mechanical properties of steel fiber-reinforced UHPC mixtures exposed to elevated temperature: effects of exposure duration and fiber content. Compos Part B 2019;168:291–301.

[13] Wille K. Concrete strength dependent pull-out behavior of deformed steel fibers. In: Joaquim AOB, editor. Proceedings pro088: 8th RILEM International Symposium on Fibre Reinforced Concrete: Challenges and Opportunities; 2012 Sep 19–21; Guimarães, Portugal. Paris: RILEM Publications SARL; 2012. p. 123–35.

[14] Tai YS, El-Tawil S. High loading-rate pullout behavior of inclined deformed steel fibers embedded in ultra-high performance concrete. Constr Build Mater 2017;148:204–18.

[15] Cao YYY, Yu QL. Effect of inclination angle on hooked end steel fiber pullout behavior in ultra-high performance concrete. Compos Struct 2018;201:151–60.

[16] Maage M. Interaction between steel fibers and cement based matrixes. Mater Constr 1977;10(5):297–301.

[17] Zhang C, Shi C, Wu Z, Ouyang X, Li K. Numerical and analytical modeling of fiber-matrix bond behaviors of high performance cement composite. Cement Concr Res 2019;125:105892.

[18] Yoo DY, Gim JY, Chun B. Effects of rust layer and corrosion degree on the pullout behavior of steel fibers from ultra-high-performance concrete. Integr Med Res 2020;9(3):3632–48.

[19] Wu Z, Khayat KH, Shi C. How do fiber shape and matrix composition affect fiber pullout behavior and flexural properties of UHPC? Cement Concr Compos 2018;90:193–201.

[20] Wille K, Naaman AE. Effect of ultra-high-performance concrete on pullout behavior of high-strength brass-coated straight steel fibers. ACI Mater J 2013;110(4):451–61.

[21] ACI Committee 544. ACI 544.9R–2017 Report on measuring mechanical properties of hardened fiber-reinforce concrete. Report. Farmington Hills: American Concrete Institute; 2017.

[22] Wu Z, Shi C, Khayat KH. Influence of silica fume content on microstructure development and bond to steel fiber in ultra-high strength cement-based materials (UHSC). Cement Concr Compos 2016;71:97–109.

[23] Wu Z, Shi C, Khayat KH. Multi-scale investigation of microstructure, fiber pullout behavior, and mechanical properties of ultra-high performance concrete with nano-CaCO₃ particles. Cement Concr Compos 2018;86:255–65.

[24] Markovic I. High-performance hybrid-fibre concrete: development and utilisation [dissertation]. Delft: Delft University of Technology; 2006.

[25] Gray RJ. Experimental techniques for measuring fibre/matrix interfacial bond shear strength. Int J Adhes Adhes 1983;3(4):197–202.

[26] Lee Y, Kang ST, Kim JK. Pullout behavior of inclined steel fiber in an ultra-high strength cementitious matrix. Constr Build Mater 2010;24(10):2030–41.

[27] Bentur A, Mindess S. Fibre reinforced cementitious composites. 2nd ed. Oxfordshire: Francis & Taylor; 2007.

[28] Kim M, Yoo DY. Cryogenic pullout behavior of steel fibers from ultra-high-performance concrete under impact loading. Constr Build Mater 2020;239:117852.

[29] Banthia N. A study of some factors affecting the fiber–matrix bond in steel fiber–reinforced concrete. Can J Civ Eng 1990;17(4):610–20.

[30] Yoo DY, Kim JJ, Park JJ. Effect of fiber spacing on dynamic pullout behavior of multiple straight steel fibers in ultra-high-performance concrete. Constr Build Mater 2019;210:461–72.

[31] Robins P, Austin S, Jones P. Pull-out behaviour of hooked steel fibres. Mater Struct 2002;35(7):434–42.

[32] Abdallah S, Fan M, Zhou X. Pull-out behaviour of hooked end steel fibres embedded in ultra-high performance mortar with various W/B ratios. Int J Concr Struct Mater 2017;11(2):301–13.

[33] Beglarigale A, Yazıcı H. Pull-out behavior of steel fiber embedded in flowable RPC and ordinary mortar. Constr Build Mater 2015;75:255–65.

[34] McSwain AC, Berube KA, Cusatis G, Landis EN. Confinement effects on fiber pullout forces for ultra-high-performance concrete. Cem Concr Compos J 2018;91:53–8.

[35] Park SH, Ryu GS, Koh KT, Kim DJ. Effect of shrinkage reducing agent on pullout resistance of high-strength steel fibers embedded in ultra-high-performance concrete. Cement Concr Compos 2014;49:59–69.

[36] Wille K, Naaman AE. Bond stress-slip behavior of steel fibers embedded in ultra high performance concrete. In: Mechtcherine V, Kaliske M, editors. In: Proceedings of the 18th European Conference on Fracture and Damage of Advanced Fiber-Reinforced Cement-Based Materials; 2010 Aug 29–Sep 3; Dresden, Germany. Zweigstelle: Aedificatio Verlag; 2010. p. 99–111.

[37] Yoo DY, Kim S, Kim JJ, Chun B. An experimental study on pullout and tensile behavior of ultra-high-performance concrete reinforced with various steel fibers. Constr Build Mater 2019;206:46–61.

[38] Chan Y, Chu S. Effect of silica fume on steel fiber bond characteristics in reactive powder concrete 2004;34:1167–72.

[39] China Association for Engineering Construction Standardization Committee. CECS13–2009: the testing method for property of bond between steel fiber and mortar. Chinese standard. Beijing: China planning press; 2009. Chinese.

[40] Deng F, Ding X, Chi Y, Xu L, Wang L. The pull-out behavior of straight and hooked-end steel fiber from hybrid fiber reinforced cementitious composite: experimental study and analytical modelling. Compos Struct 2018;206:693–712.

[41] Qi J, Wu Z, Ma ZJ, Wang J. Pullout behavior of straight and hooked-end steel fibers in UHPC matrix with various embedded angles. Constr Build Mater 2018;191:764–74.

[42] Gray RJ. Analysis of the effect of embedded fibre length on fibre debonding and pull-out from an elastic matrix-part 2 application to a steel fibre-cementitious matrix composite system. J Mater Sci 1984;19(5):1680–91.

[43] Bartos P. Review paper: bond in fibre reinforced cements and concretes. Int J Cem Compos Light Concr 1981;3(3):159–77.

[44] Beaumont PWR, Aleszka JC. Cracking and toughening of concrete and polymer-concrete dispersed with short steel wires. J Mater Sci 1978;13(8):1749–60.

[45] Wu Z, Shi C, Khayat KH, Wan S. Effects of different nanomaterials on hardening and performance of ultra-high strength concrete (UHSC). Cement Concr Compos 2016;70:24–34.

[46] Wu Z, Khayat KH, Shi C. Effect of nano-SiO2 particles and curing time on development of fiber–matrix bond properties and microstructure of ultra-high strength concrete. Cement Concr Res 2017;95:247–56.

[47] Scrivener KL, Crumbie AK, Laugesen P. The interfacial transition zone (ITZ) between cement paste and aggregate in concrete. Interface Sci 2004;12(4):411–21.

[48] Frazão C, Barros J, Camões A, Alves AC, Rocha L. Corrosion effects on pullout behavior of hooked steel fibers in self-compacting concrete. Cement Concr Res 2016;79:112–22.

[49] Yoo DY, Kim JJ, Chun B. Dynamic pullout behavior of half-hooked and twisted steel fibers in ultra-high-performance concrete containing expansive agents. Compos, Part B Eng 2019;167:517–32.

[50] Kang ST, Kim JK. The relation between fiber orientation and tensile behavior in an ultra high performance fiber reinforced cementitious composites (UHPFRCC). Cement Concr Res 2011;41(10):1001–14.

[51] Alwan JM, Naaman AE, Guerrero P. Effect of mechanical clamping on the pull-out response of hooked steel fibers embedded in cementitious matrices. Mater Struct 1999;1:15–25.

[52] Pompo A, Stupak PR, Nicolais L, Marchese B. Analysis of steel fibre pull-out from a cement matrix using video photography. Cement Concr Compos 1996;18(1):3–8.

[53] Abdallah S, Fan M, Rees DWA. Analysis and modelling of mechanical anchorage of 4D/5D hooked end steel fibres. Mater Des 2016;112:539–52.

[54] Isla F, Ruano G, Luccioni B. Analysis of steel fibers pull-out. Experimental study. Constr Build Mater 2015;100:183–93.

[55] Zīle E, Zīle O. Effect of the fiber geometry on the pullout response of mechanically deformed steel fibers. Cement Concr Res 2013;44:18–24.

[56] Chanvillard G, Aïtcin PC. Pull-out behavior of corrugated steel fibers: qualitative and statistical analysis. Adv Cement Base Mater 1996;4(1):28–41.

[57] American Society for Testing and Materials (ASTM). C1856/C1856M-17: standard practice for fabricating and testing specimens of ultra-high performance. West Conshohocken: ASTM International; 2017.

[58] Kim JJ, Kim DJ, Kang ST, Lee JH. Influence of sand to coarse aggregate ratio on the interfacial bond strength of steel fibers in concrete for nuclear power plant. Nucl Eng Des 2012;252:1–10.

[59] Wille K, Naaman AE. Pullout behavior of high-strength steel fibers embedded in ultra-high-performance concrete. ACI Mater J 2012;109:479–88.

[60] Chun B, Yoo DY, Banthia N. Achieving slip-hardening behavior of sanded straight steel fibers in ultra-high-performance concrete. Cement Concr Compos 2020;113:103669.

[61] Feng J, Sun WW, Wang XM, Shi XY. Mechanical analyses of hooked fiber pullout performance in ultra-high-performance concrete. Constr Build Mater 2014;69:403–10.

[62] Tai YS, El-Tawil S, Chung TH. Performance of deformed steel fibers embedded in ultra-high performance concrete subjected to various pullout rates. Cement Concr Res 2016;89:1–13.

[63] Abdallah S, Fan M. Anchorage mechanisms of novel geometrical hooked-end steel fibres. Mater Struct Constr 2017;50(2):139.

[64] Cox HL, M.A., Ae.S FR, Mech.E AMI. The elasticity and strength of paper and other fibrous materials. Br J Appl Phys 1952;3(3):72–9.

[65] Chen X, Beyerlein IJ, Brinson LC. Curved-fiber pull-out model for nanocomposites. Part 1: bonded stage formulation. Mech Mater 2009;41(3):279–92.

[66] Nairn JA. On the use of shear-lag methods for analysis of stress transfer in unidirectional composites. Mech Mater 1997;26(2):63–80.

[67] Gao X, Li K. A shear-lag model for carbon nanotube-reinforced polymer composites. Int J Solids Struct 2005;42(5–6):1649–67.

[68] Rosen BW. Tensile failure of fibrous composites. AIAA J 1964;2(11):1985–91.

[69] Lawrence P. Some theoretical considerations of fibre pull-out from an elastic matrix variation of fibre load. J Mater Sci 1972;7(1):1–6.

[70] Wang Y, Li VC, Backer S. Modelling of fibre pull-out from a cement matrix. Int J Cem Compos Light Concr 1988;10(3):143–9.

[71] Naaman AE, Namur GG, Alwan JM, Najm HS. Fiber pullout and bond slip. I: analytical study. J Struct Eng 1991;117(9):2769–90.

[72] Naaman AE, Namur GG, Alwan JM, Najm HS. Fiber pullout and bond slip. II: experimental validation. J Struct Eng 1991;117(9):2791–800.

[73] Gao YC, Mai YW, Cotterell B. Fracture of fiber-reinforced materials. Z Angew Math Phys 1988;39(4):550–72.

[74] Li VC, Chan YW. Determination of interfacial debond mode for fiber-reinforced cementitious composites. J Eng Mech 1994;120(4):707–19.

[75] Kim JK, Baillie C, Mai YW. Interfacial debonding and fibre pull-out stresses. Part I critical comparison of existing theories with experiments. J Mater Sci 1992;27(12):3143–54.

[76] Zhan Y, Meschke G. Analytical model for the pullout behavior of straight and hooked-end steel fibers. J Eng Mech 2014;140(12):04014091.

[77] Chanvillard G. Modeling the pullout of wire-drawn steel fibers. Cement Concr Res 1999;29(7):1027–37.

[78] Soetens T, Van Gysel A, Matthys S, Taerwe L. A semi-analytical model to predict the pull-out behaviour of inclined hooked-end steel fibres. Constr Build Mater 2013;43:253–65.

[79] Cunha VMCF, Barros JAO, Sena-cruz J. Analytical model for bond-slip of hooked-end steel fibers. In: Barros J, Ferreira AM, editors. Proceedings of the International Conference Challenges for Civil Construction |e Bridge Science and Applications with Engineering Towards Innovative Solutions: Safety, Sustainability and Rehabilitation With Innovative Solutions; 2008 Apr 16–18; Porto, Portugal. Porto: FEUP Edições; 2008. p. 1–12.

[80] Abdallah S, Rees DWA. Comparisons between pull-out behaviour of various hooked-end fibres in normal–high strength concretes. Int J Concr Struct Mater 2019;13:27.

[81] Sujivorakul C, Waas AM, Naaman AE. Pullout response of a smooth fiber with an end anchorage. J Eng Mech 2000;126(9):986–93.

[82] Ghoddousi P, Ahmadi R, Sharifi M. Fiber pullout model for aligned hooked-end steel fiber. Can J Civ Eng 2010;37(9):1179–88.

[83] Won J, Lee J, Lee S. Predicting pull-out behaviour based on the bond mechanism of arch-type steel fibre in cementitious composite. Compos Struct 2015;134:633–44.

[84] Zhang H, Ji T, Lin X. Pullout behavior of steel fibers with different shapes from ultra-high performance concrete (UHPC) prepared with granite powder under different curing conditions. Constr Build Mater 2019;211:688–702.

[85] Yoo DY, Choi HJ, Kim S. Bond-slip response of novel half-hooked steel fibers in ultra-high-performance concrete. Constr Build Mater 2019;224:743–61.

[86] Chun B, Yoo DY. Hybrid effect of macro and micro steel fibers on the pullout and tensile behaviors of ultra-high-performance concrete. Compos Part B Eng 2019;162:344–60.

[87] Banthia N, Trottier J. Concrete reinforced with deformed steel fibers, part I : bond-slip mechanisms. ACI Mater J 1994;91(5):435–46.

[88] Kim JJ, Yoo DY. Effects of fiber shape and distance on the pullout behavior of steel fibers embedded in ultra-high-performance concrete. Cement Concr Compos 2019;103:213–23.

[89] Xu M, Hallinan B, Wille K. Effect of loading rates on pullout behavior of high strength steel fibers embedded in ultra-high performance concrete. Cement Concr Compos 2016;70:98–109.

[90] Abu-Lebdeh T, Hamoush S, Heard W, Zornig B. Effect of matrix strength on pullout behavior of steel fiber reinforced very-high strength concrete composites. Constr Build Mater 2011;25(1):39–46.

[91] Yoo DY, Chun B, Kim JJ. Bond performance of abraded arch-type steel fibers in ultra-high-performance concrete. Cement Concr Compos 2020;109:103538.

[92] Chin CS, Xiao RY. Experimental and nonlinear finite element analysis of fiber-cementitious matrix bond-slip mechanism. High Perform Fiber Reinf Cem Compos 2012;2:145–52.

[93] Kang ST, Lee BY, Kim JK, Kim YY. The effect of fibre distribution characteristics on the flexural strength of steel fibre-reinforced ultra high strength concrete. Constr Build Mater 2011;25(5):2450–7.

[94] Cunha MCF. Steel fibre reinforced self-compacting concrete (from micro-mechanics to composite behaviour) [dissertation]. Braga: University of Minho; 2010.

[95] Yoo DY, Park JJ, Kim SW. Fiber pullout behavior of HPFRCC: effects of matrix strength and fiber type. Compos Struct 2017;174:263–76.

[96] Yang L, Shi C, Wu Z. Mitigation techniques for autogenous shrinkage of ultra-high-performance concrete—a review. Compos Part B 2019;178:107456.

[97] Park SH, Kim DJ, Ryu GS, Koh KT. Tensile behavior of ultra high performance hybrid fiber reinforced concrete. Cement Concr Compos 2012;34(2):172–84.

[98] Zhang Y, Zhu Y, Qu S, Kumar A, Shao X. Improvement of flexural and tensile strength of layered-casting UHPC with aligned steel fibers. Constr Build Mater 2020;251:118893.

[99] Wu Z, Shi C, He W, Wang D. Static and dynamic compressive properties of ultra-high performance concrete (UHPC) with hybrid steel fiber reinforcements. Cement Concr Compos 2017;79:148–57.

[100] Abdallah S, Fan M, Cashell KA. Bond-slip behaviour of steel fibres in concrete after exposure to elevated temperatures. Constr Build Mater 2017;140:542–51.

[101] Kim MJ, Yoo DY. Analysis on enhanced pullout resistance of steel fibers in ultra-high performance concrete under cryogenic condition. Constr Build Mater 2020;251:118953.